

# Flipping Out: Role of Arginine in Hydrophobic Polymer Collapse

Jonathan W. P. Zajac,<sup>†</sup> Praveen Muralikrishnan,<sup>‡</sup> Caryn L. Heldt,<sup>¶</sup> Sarah L.  
Perry,<sup>§</sup> and Sapna Sarupria<sup>\*,†</sup>

<sup>†</sup>*Department of Chemistry, University of Minnesota, Minneapolis, MN 55455, USA*

<sup>‡</sup>*Department of Chemical Engineering and Materials Science, University of Minnesota,  
Minneapolis, MN 55455, USA*

<sup>¶</sup>*Department of Chemical Engineering, Michigan Technological University, Houghton, MI  
49931, USA*

<sup>§</sup>*Department of Chemical Engineering, University of Massachusetts Amherst, MA 01003,  
USA*

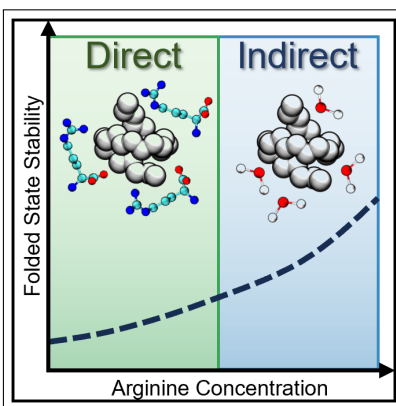
<sup>||</sup>*Chemical Theory Center, University of Minnesota, Minneapolis, MN 55455, USA*

E-mail: sarupria@umn.edu

## Abstract

Arginine has been a mainstay in biological formulation development for decades. To date, the way arginine modulates protein stability has been widely studied and debated. Here, we employed a hydrophobic polymer to decouple hydrophobic effects from other interactions relevant to protein folding. While existing hypotheses for the effects of arginine can generally be categorized as either direct or indirect, our results indicate that direct and indirect mechanisms of arginine co-exist and oppose each other. At low concentrations, arginine was observed to stabilize hydrophobic polymer collapse via a sidechain-dominated direct mechanism, while at high concentrations, arginine stabilized polymer collapse via a backbone-dominated indirect mechanism. These findings highlight the modular nature of the widely used additive arginine, with relevance in the design of stable biological formulations.

## TOC Graphic



## Keywords

Hydrophobic interactions, formulation design, excipient, osmolyte, protein stability, protein folding

Maintaining native protein structures in biological formulations poses a challenge, and is commonly addressed by strategic additive incorporation.<sup>1-3</sup> Arginine stands out as a frequently employed additive in such formulations, spanning both therapeutic proteins<sup>4</sup> and vaccines.<sup>5,6</sup> Arginine has been widely used as an aggregation suppressor, an agent for protein refolding, a cryoprotectant during lyophilization, and in protein purification.<sup>7-9</sup> Once hailed as a universal stabilizer, emerging studies paint a foggier picture of the effects of arginine. In some settings, the presence of arginine has accelerated the aggregation,<sup>10-12</sup> denaturation,<sup>13-15</sup> and inactivation<sup>16</sup> of certain proteins and viruses. Additional studies have found that arginine increases or decreases protein melting temperature depending on concentration.<sup>17,18</sup> Hence, the existing literature on arginine reveals a lack of a cohesive understanding of its multifaceted effects on protein stability.

The molecular mechanism for arginine effects on protein stability remains elusive. In general, additive effects on protein stability are thought to be either direct or indirect. Direct mechanisms involve direct protein-additive interactions that drive stabilization, while indirect mechanisms influence protein stability by modulating the surrounding solvent structure. It remains debated whether arginine acts primarily via a direct or indirect mechanism. Several studies called attention to direct interactions between arginine and aromatic residues,<sup>7,19,20</sup> acidic residues,<sup>12,17</sup> and hydrophobic moieties.<sup>21,22</sup> Other studies have proposed clusters of free arginine molecules in solution enable the crowding out of protein-protein interactions,<sup>17,20,23,24</sup> or alteration of hydration shell water dynamics.<sup>25,26</sup> The wide range of observations related to the role of arginine on protein stability suggests that arginine harbors diverse, context-dependent mechanisms.

To elucidate the mechanisms through

which arginine influences protein stability, this study focuses on its effects on hydrophobic interactions. Hydrophobic interactions are key in several biologically relevant phenomena, including protein folding and stability.<sup>27-35</sup> Additives in solutions have been observed to modulate the strength of hydrophobic interactions, and in turn, the stability of proteins.<sup>36-42</sup> For example, simulation studies have shown that trimethylamine N-oxide (TMAO) has a negligible effect on or strengthens hydrophobic interactions,<sup>38,43-47</sup> while hydrophobic interactions are weakened in urea solutions.<sup>37,39,40,48-52</sup> Indeed, the effects of urea and TMAO on hydrophobic interactions are consistent with their experimentally-observed roles as a protein denaturant and stabilizer, respectively.<sup>41,53-55</sup>

Molecular dynamics (MD) simulations have provided valuable insights towards understanding these mechanisms as they relate to hydrophobicity. Several studies have highlighted the utilization of a hydrophobic polymer model for describing the role of solvent and additives on protein-like collapse.<sup>39,40,56-59</sup> The use of a hydrophobic polymer model enables the decoupling of additive effects on hydrophobic vs other interactions, which is challenging in experiments. In the present study, we utilize MD simulations of a hydrophobic polymer to characterize the effects of arginine on many-body hydrophobic interactions pertinent to protein stability.

We simulated a hydrophobic polymer in arginine solutions at different concentrations (Table S2). Replica exchange umbrella sampling<sup>60</sup> (REUS) simulations were performed using GROMACS 2021.4<sup>61,62</sup> with the PLUMED 2.8.0<sup>63,64</sup> patch applied. The hydrophobic polymer was modeled as a linear coarse-grained chain with 26 monomers, where each monomer represents a CH<sub>2</sub> unit with Lennard-Jones parameters  $\sigma = 0.373$  nm and  $\epsilon = 0.5856$  kJ/mol.<sup>38</sup> Chloride (Cl<sup>-</sup>)

counterions were added to achieve charge neutrality. The TIP4P/2005<sup>65</sup> model was used to describe water, and the CHARM22 force field was used for arginine and Cl<sup>-</sup>.<sup>66</sup> Lorentz-Berthelot mixing rules<sup>67</sup> were used to calculate non-bonded interactions between different atom types, except for polymer-water oxygen interactions (see SI for details).

The potential of mean force (PMF) along the radius of gyration of the polymer was calculated as  $W(R_g) = -k_B T \ln(P(R_g))$ . Biased probability distributions were reweighted according to the Weighted Histogram Analysis Method (WHAM).<sup>68</sup> The free energy of polymer unfolding ( $\Delta G_u$ ) was calculated according to:

$$\exp\left(\frac{\Delta G_u}{k_B T}\right) = \frac{\int_{R_{g,cut}}^{R_{g,max}} \exp\left(\frac{-W(R_g)}{k_B T}\right) dR_g}{\int_{R_{g,min}}^{R_{g,cut}} \exp\left(\frac{-W(R_g)}{k_B T}\right) dR_g} \quad (1)$$

where  $R_{g,cut}$  was determined as the point between the folded and unfolded states where  $\frac{\partial W(R_g)}{\partial R_g} = 0$ .

Fig. 1a shows the PMF along the  $R_g$  reaction coordinate. In all solutions, free energy minima were observed at approximately 0.4 and 0.8 nm (labeled as III in Fig. 1g), along with a prominent free energy barrier at  $\sim 0.6$  nm representing the transition between folded and unfolded states. (Fig. 1a). In pure water, hydrophobic collapse is unfavorable, with the unfolded state favored by  $\sim 0.3$  kT. In contrast, at all arginine concentrations, the folded state of the polymer is favored relative to pure water, and a monotonic increase in  $\Delta G_u$  is observed (Fig. S4). An additional barrier at  $\sim 0.45$  nm was identified separating two folded states, labeled as I and II in Fig. 1a.

The folded polymer ensemble in arginine solutions exhibits free energy minima corre-

sponding to globular ( $\sim 0.4$  nm) and hairpin-like ( $\sim 0.5$  nm) configurations (Fig. 1g). Arginine clusters encapsulating the hydrophobic polymer are observed in each state (Fig. S6). We propose that the free energy barrier separating these two states arises from an energetic penalty associated with breaking these encapsulating clusters. Such a mechanism is similar to that observed by Li et al.,<sup>22</sup> who observed arginine-mediated suppression of hydrophobic association.

The PMF was decomposed into individual components to further investigate the role of arginine in polymer collapse. Following the methods outlined by several others,<sup>42,69-71</sup> the PMF was decomposed as

$$W(R_g) = W_{vac}(R_g) + W_{cav}(R_g) + E_{pw}(R_g) + E_{pa}(R_g) + E_{pc}(R_g) \quad (2)$$

$W_{vac}(R_g)$  captures intrapolymer degrees of freedom and was obtained from independent REUS simulations of the polymer in vacuum.  $E_{pw}(R_g)$ ,  $E_{pa}(R_g)$ , and  $E_{pc}(R_g)$  are average polymer-water, polymer-arginine, and polymer-chloride interaction energies, respectively. The remaining term is  $W_{cav}(R_g)$ , which is the cavitation component and quantifies the energetic cost of forming a cavity – of the same size and shape as the polymer – in the solution.

Fig. 1b-f shows the decomposition of the PMF into these various components. The vacuum component favors the folded state of the polymer, associated with favorable intrapolymer interactions and configurational entropy upon collapse (Fig. 1b). Because this component does not depend on the presence of arginine, a balance of the remaining components dictates the effect of arginine on hydrophobic polymer collapse.

Near large idealized solutes or hydrophobic interfaces, water dewets and forms a vapor-liquid-like interface.<sup>72,73</sup> Similar behav-

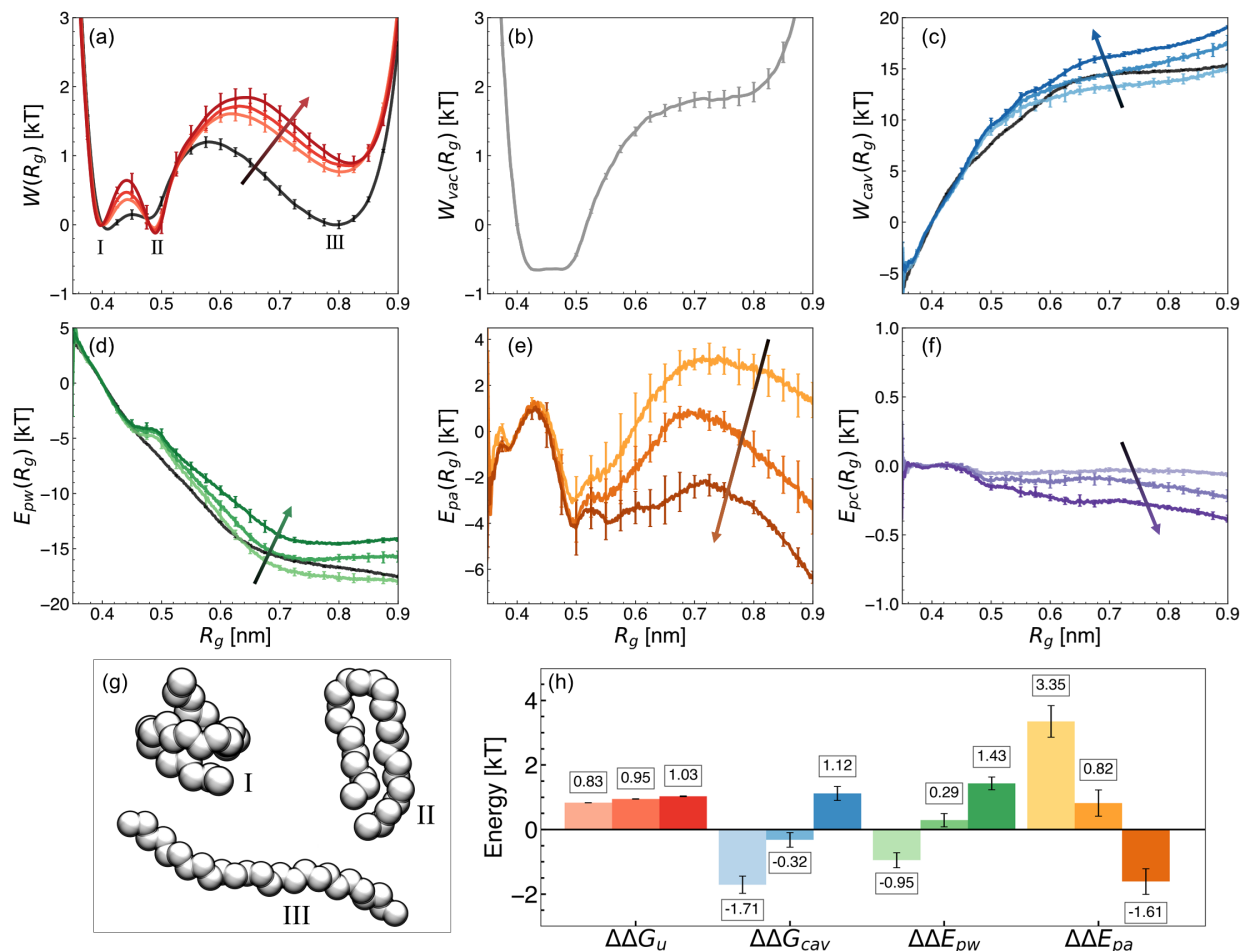


**Figure 1:** PMF decomposition in 0.0 M, 0.25 M, 0.5 M, and 1.0 M arginine solutions. (a) The PMF obtained along the  $R_g$  reaction coordinate,  $W(R_g)$ , (b) vacuum contribution,  $W_{vac}$ , (c) cavitation contribution,  $W_{cav}$ , (d) polymer-water interactions,  $E_{pw}$ , (e) polymer-arginine interactions,  $E_{pa}$ , and (f) polymer-chloride interactions,  $E_{pc}$ . (g) Representative configurations along the reaction coordinate as denoted in (a) as I, II, and III. (h) Changes in overall free energy of unfolding ( $\Delta\Delta G_u$ ), cavitation contribution ( $\Delta\Delta G_{cav}$ ), polymer-water interactions ( $\Delta\Delta E_{pw}$ ), and polymer-arginine interactions ( $\Delta\Delta E_{pa}$ ). Increasing arginine concentration is denoted by increased shading (light to dark) and is indicated by arrows in (a-f). The polymer in water alone is shown in black, where appropriate. Mean values were estimated from three replicate REUS simulations. Error bars are reported as described in the SI. All plots are normalized to 0 at  $R_g = 0.4$  nm, where appropriate.

ior may be expected for our hydrophobic polymer; hence, we computed  $W_{cav}$ , which depends on both the size and shape of the polymer and is related to the air-water surface tension.<sup>69,70,74</sup> The cavitation component favors the folded state (Fig. 1c), reflecting a strong hydrophobic driving force for polymer

collapse.<sup>56</sup>

Attractive polymer-water interactions become more favorable with increasing  $R_g$  (Fig. 1d), indicating polymer-water attractive interactions oppose polymer collapse. It is worth noting that the free energy minima at  $\sim 0.8$  nm in the unfolded ensemble is ob-

served in an aqueous environment (Fig. 1a), but not in vacuum (Fig. 1b). This minima arises due to favorable polymer-water interactions, consistent with prior MD simulations that observed water-mediated interactions drive large hydrophobic solutes apart.<sup>57,75,76</sup> Additionally, sufficient dewetting of the hydrophobic polymer is a known bottleneck to collapse,<sup>56,69,77</sup> resulting in the free energy barrier at  $\sim 0.6$  nm separating the folded and unfolded states.

Attractive polymer-arginine interactions approach an energetic minima at  $\sim 0.5$  nm (Fig. 1e), giving rise to the global minimum observed in the overall PMF. Polymer-chloride interactions were observed on the order of thermal fluctuations ( $< 0.5$  kT), consistent with previous observations that chloride ions are depleted from the local domain of hydrophobic solutes.<sup>37,78</sup>

Fig. 1h shows the change in each component upon unfolding in arginine solution relative to that observed in water. In Fig. 1h, the first  $\Delta$  arises from the difference between folded and unfolded states (e.g.,  $\Delta E = \langle E_u \rangle - \langle E_f \rangle$ ), and the second  $\Delta$  arises from the free energy difference between arginine solution ( $\Delta E_{arg}$ ) and water ( $\Delta E_{wat}$ ) (e.g.,  $\Delta\Delta E = \Delta E_{arg} - \Delta E_{wat}$ ). With increasing arginine concentration, we observed an increasingly favorable cavitation component (Fig. 1h). Lin and Timasheff<sup>79</sup> previously connected protein stability with cavity formation and vapor-liquid surface tension. They proposed that the expansion of a protein-containing cavity requires more energy in the presence of an additive that increases surface tension at the cavity-solution interface. Experimentally, increasing arginine concentration has been observed to increase the vapor-liquid surface tension of aqueous solutions,<sup>80</sup> which may explain the dependence of  $\Delta\Delta G_{cav}$  observed in the present study.

Looking at the trends in  $\Delta\Delta E_{pw}$ , we found that in 0.25 M arginine solutions, the

polymer-water component favors polymer unfolding relative to in pure water (Fig. 1h). At 0.5 M and 1.0 M arginine concentrations, this component favors polymer collapse. With arginine present, the local domain of the polymer exhibits a reduction in the average number of water molecules (Fig. S10), indicating an effective expulsion of water. This, in turn, diminishes polymer-water interactions that resist polymer collapse.

The polymer-arginine contribution is observed to favor the folded polymer state at 0.25 M and 0.5 M arginine concentrations relative to in pure water (Fig. 1h). However, at 1.0 M arginine concentrations, polymer-arginine interactions promote polymer unfolding. The fact that high concentrations of arginine favored polymer unfolding is evidence that the direct mechanism of arginine-induced stabilization cannot fully explain the effect of this additive on hydrophobic polymer collapse.

To investigate potential competing effects of direct and indirect mechanisms, we combined the components of our PMF decomposition, delineating between those linked to direct effects (polymer-arginine and polymer-chloride;  $\Delta\Delta G_{dir}$ ) and indirect effects (cavitation and polymer-water;  $\Delta\Delta G_{ind}$ ) of arginine (Fig. 2a).

We discovered that, with increasing concentration, the mechanism underlying the effects of arginine transitions from direct to indirect dominance. At 0.25 M, cavity formation and polymer-water interactions oppose polymer collapse, while arginine-polymer interactions favor collapse. The balance of these components gives rise to  $\Delta\Delta G_{dir} > \Delta\Delta G_{ind}$ , resulting in net stabilization of folded conformations and supporting the direct mechanism hypothesis (Fig. 2a).

In contrast, for the high-concentration regime (0.5 M and 1.0 M), cavity formation and polymer-water attractive interactions favor polymer collapse, while attractive

arginine-polymer interactions favor extension of the hydrophobic polymer. In this case, indirect components dominated the free energy difference ( $\Delta\Delta G_{dir} < \Delta\Delta G_{ind}$ ), stabilizing the polymer collapse and supporting the indirect hypothesis (Fig. 2a).

Thus, within the range of concentrations studied, we have uncovered that arginine exists at the edge of a mechanistic flip between direct- and indirect-dominated stabilization of many-body hydrophobic interactions. The identification of this mechanistic switch may explain the wide variety of hypotheses in the existing arginine literature. Because arginine is situated on this razor’s edge, small changes associated with the chemistry of a protein surface, the addition of cosolvents to

solution, or differences in sample preparation, may cause significant changes in the modulation of hydrophobic interactions due to arginine.

Arginine is comprised of a polar backbone and an aliphatic side chain characterized by a guanidinium group. To investigate the roles of these components on hydrophobic polymer collapse, we completed an additional PMF decomposition in guanidinium and glycine solutions (see SI for simulation details). At all concentrations under study, we observed that guanidinium favors the hydrophobic polymer collapse primarily via a direct mechanism, while glycine stabilizes polymer collapse primarily via an indirect mechanism (Fig. 2b,c).

In the case of guanidinium, stabiliza-

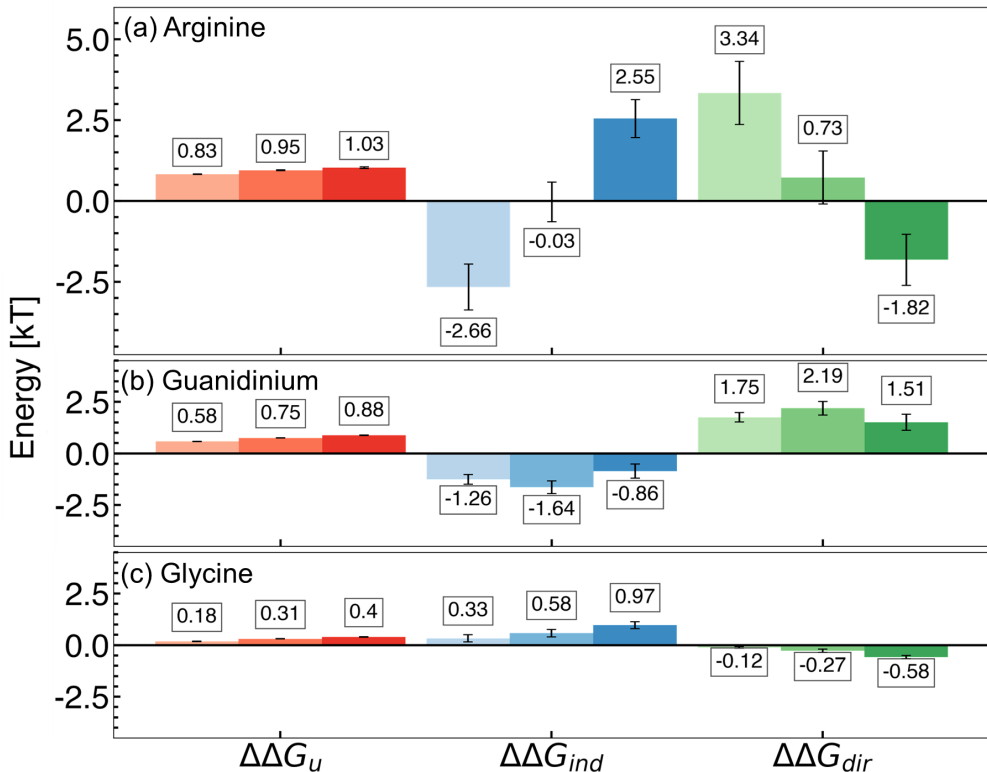


**Figure 2:** Contributions to the free energy of hydrophobic polymer unfolding in 0.25 M, 0.50 M, and 1.0 M (a) arginine, (b) guanidinium, and (c) glycine solutions. Changes in overall free energy of unfolding ( $\Delta\Delta G_u$ ), direct interactions ( $\Delta\Delta G_{dir}$ ), and indirect interactions ( $\Delta\Delta G_{ind}$ ) and polymer are shown. Increasing additive concentration is denoted by increased shading (light to dark; left to right). Mean values are reported from three replicate REUS simulations. Error bars were estimated via error propagation (see SI for details).

tion is driven entirely by attractive polymer-guanidinium interactions that favor collapse, while polymer-water interactions and cavity formation oppose polymer folding (Fig. 2b). In glycine solutions, however, stability is driven by the inverse mechanism; polymer-water interactions and the cavitation component favor collapse, while folding is opposed by attractive polymer-glycine interactions (Fig. 2c). Based on these findings, we characterize arginine as exhibiting a guanidinium-like mechanism at low concentrations and a glycine-like mechanism at high concentrations.

While glycine is known to be an effective stabilizer of proteins,<sup>18,81,82</sup> our observations obtained for guanidinium are somewhat surprising due to its common role as a protein denaturant.<sup>83-85</sup> Several studies have stressed the importance of direct interactions in guanidinium-induced denaturation, primarily via breaking salt bridges, competing for intra-protein hydrogen bonds, and interacting with aromatic moieties via cation- $\pi$  stacking.<sup>84,86,87</sup> Usually, this occurs at high concentrations of guanidinium salts. Our findings suggest that while guanidinium may stabilize hydrophobic interactions at low concentrations, this is outweighed by the denaturation mechanisms at high concentrations.

Thermodynamic analyses of arginine effects on polymer collapse discussed above indicate that direct and indirect mechanisms co-exist and compete at all concentrations under study. To probe this further, we characterize the molecular interactions between arginine, water, and the polymer. Specifically, we look at hydrogen bonding between arginine and water to characterize arginine-water interactions. Preferential interactions are used to elucidate polymer-arginine-water interactions.

Fig. 3 describes hydrogen bonding interactions between arginine and water. Hydrogen bonds were calculated according to geo-

metric criteria of a donor-acceptor distance of  $r \leq 0.35$  nm and an angle deviating less than  $30^\circ$  from  $180^\circ$ .<sup>88</sup> Hydrogen bond existence correlation functions for water-water, guanidinium-water, carboxylate-water, and amine-water were estimated according to<sup>89-91</sup>

$$C(\tau) = \left\langle \frac{\sum_{i,j} h_{ij}(t_0)h_{ij}(t_0 + \tau)}{\sum_{i,j} h_{ij}(t_0)^2} \right\rangle \quad (3)$$

where  $h_{ij}(t_0)$  is equal to 1 if there is a hydrogen bond between groups  $i$  and  $j$  at time  $t_0$ , and 0 if no hydrogen bond is present. An average over all possible values of the time origin  $t_0$  was taken over the last 5 ns of 20 ns equilibrium simulations.

Overall, the number of backbone-water hydrogen bonds was observed to be greater than sidechain-water hydrogen bonds (Fig. 3a). We further observed the fraction of occupied hydrogen bonding sites to be higher for backbone groups than the sidechain (Fig. S7). The hydrogen bond existence autocorrelation function for the 0.25 M arginine solution revealed hydrogen bonds formed between backbone-water atoms are, on average, longer-lived than sidechain-water hydrogen bonds (Fig. 3b). As arginine concentration was increased, hydrogen bond lifetimes were also observed to increase for both arginine-water and water-water interactions (Fig. S8).

Pairwise radial distribution functions (RDFs) were computed between the water oxygen (OW) and either the alpha carbon (CA) or guanidinium carbon (CZ) of arginine to quantify the local structure of water around arginine molecules (Fig. 3c). The first peak in the OW-CA RDF was observed to increase slightly with concentration. This indicates preferential hydration of the backbone as more arginine molecules are introduced to the solution. There is, however, no such change observed in the OW-CZ RDF with concentration. A representative snap-



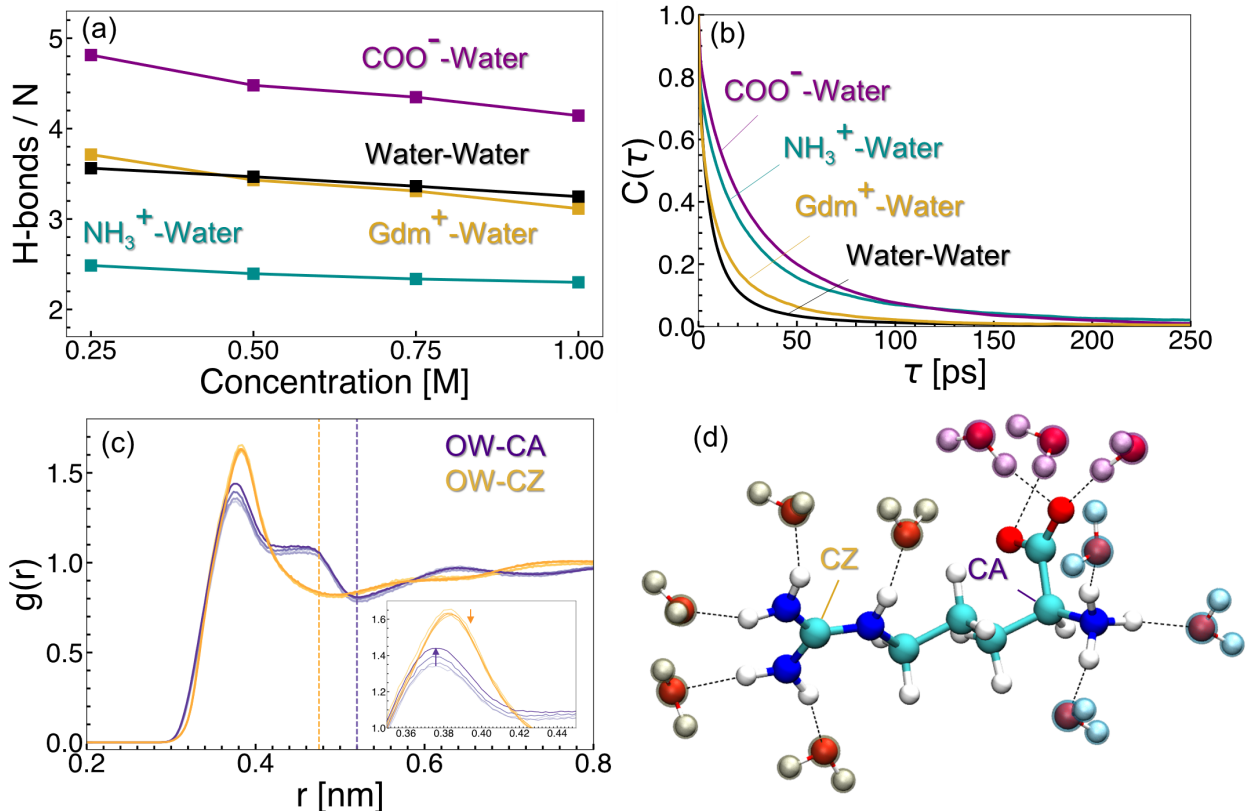


**Figure 3:** Arginine-water interactions. (a) Hydrogen bonds observed between backbone groups ( $\text{COO}^-$ ,  $\text{NH}_3^+$ ) and the guanidinium ( $\text{Gdm}^+$ ) sidechain with water. (b) Hydrogen bond existence correlation functions for water-water,  $\text{COO}^-$ -water,  $\text{Gdm}^+$ -water, and  $\text{NH}_3^+$ -water. (c) Radial distribution function between OW and either CA (purple) or CZ (gold). (c, inset) Arrows denote trends observed with increasing arginine concentration. (d) A representative snapshot of hydrogen-bonding interactions involving arginine and water. Water molecules interacting with the  $\text{Gdm}^+$  sidechain are highlighted in yellow, while those interacting with  $\text{NH}_3^+$  and  $\text{COO}^-$  are shaded in blue and purple, respectively.

shot of the hydration shell of a single arginine molecule is shown in Fig. 3d (2D representation is shown in Fig. S9). Together, these results indicate that the backbone of arginine interacts favorably with water.

While we found arginine preferentially interacts with water via its backbone, we hypothesized arginine interacts with the polymer via its sidechain. It has been reported elsewhere that dehydration of the guanidinium face is important in forming face-face stacking interactions in aqueous guanidinium solutions.<sup>92</sup> In our case, the dehydrated face

of guanidinium is expected to play a key role in direct arginine-polymer interactions, similar to interactions observed between guanidinium and hydrophobic/aromatic protein residues.<sup>7,19,20,93</sup>

Distribution of arginine with respect to the polymer is described via the preferential interaction coefficient ( $\Gamma_{PA}$ ),<sup>94-96</sup>

$$\Gamma_{PA} = - \left( \frac{\partial \mu_P}{\partial \mu_A} \right)_{m_P, T, P} = \left( \frac{\partial m_A}{\partial m_P} \right)_{\mu_A, T, P} \quad (4)$$

where  $\mu$  is the chemical potential,  $m$  is the concentration and  $W$ ,  $P$ , and  $A$  refer to wa-

ter, polymer, and the additive, respectively. This parameter is calculated in simulations using the two-domain formula<sup>97-99</sup> given by,

$$\Gamma_{PA} = \left\langle N_A^{\text{local}} - \left( \frac{N_A^{\text{bulk}}}{N_W^{\text{bulk}}} \right) N_W^{\text{local}} \right\rangle \quad (5)$$

where  $N$  represents the number of molecules of a given species and angular brackets denote an ensemble average. The local and bulk domain was separated by a cutoff distance  $R_{\text{cut}}$  from the polymer.  $\Gamma_{PA}$  gives a measure of the relative accumulation or depletion of an additive in the local domain of the hydrophobic polymer, with  $\Gamma_{PA} > 0$  indicating relative accumulation (preferential interaction) and  $\Gamma_{PA} < 0$  indicating relative depletion (preferential exclusion).

Wyman-Tanford theory relates the dependence of any equilibrium process (such as protein folding) and preferential interaction as:<sup>100-102</sup>

$$-\left( \frac{\partial \Delta G^u}{\partial \mu_A} \right) = \Gamma_{PA}^u - \Gamma_{PA}^f \quad (6)$$

As a result, denaturants are expected to have a greater preferential interaction coefficient in the unfolded ensemble, while stabilizing osmolytes have a greater preferential interaction coefficient in the folded ensemble.<sup>41,58,103,104</sup> In 0.25 M arginine concentration, we observed greater preferential interactions with the folded state relative to the unfolded state (Fig. 4a; Fig. S11a-c). With increasing concentration, we observe a diminishing difference between  $\Gamma_{PA}^u$  and  $\Gamma_{PA}^f$ , in line with the mechanistic flip from a direct- to indirect-dominated stabilization mechanism.

Preferential interaction coefficients for guanidinium and glycine solutions are shown in Fig. 4b and c, respectively. We observed that at all concentrations, guanidinium preferentially interacts with the hydrophobic polymer (Fig. 4b). This is consistent with experimental evidence, as well as a

prior simulation study that observed attractive guanidinium-polymer interactions for a model hydrophobic polymer.<sup>39,70</sup> Glycine, meanwhile, was found to be preferentially excluded from the local domain of the hydrophobic polymer (Fig. 4c). This finding is consistent with the observed preference for the backbone of arginine to hydrogen bond with water, relative to the sidechain. Elsewhere, glycine has been observed to deplete from the surface of several model miniproteins, consistent with our findings.<sup>104</sup>

To explore whether the preferential interactions of arginine with polymer and water are accompanied by preferential orientations, we computed an orientation parameter inspired by Shukla and Trout.<sup>105</sup> This parameter was computed as the angle formed in three-dimensional space between polymer-CZ and CZ-CA vectors (Fig. 5a). The monomer closest to CZ is taken for the polymer-CZ vector. Angles where  $\theta > 90^\circ$  indicate the arginine backbone orients towards the bulk solvent, while  $\theta < 90^\circ$  indicates the arginine backbone orients towards the polymer. We observed that for all concentrations, the probability  $P(\theta)$  is skewed towards angles greater than  $90^\circ$  (Fig. 5b-d).

Further, for all arginine concentrations, the mean value of  $\theta$  for the folded state is greater than that observed for unfolded configurations (Fig. 5b-d). This preferential orientation of arginine enables the hydrophobic face of the guanidinium sidechain to interact with the hydrophobic polymer, while extension of the backbone towards the bulk enables additional interactions with either water or other free arginine molecules. The greater ability for arginine to adopt preferred orientations in the folded state, particularly at 0.25 M, may partially explain the favorable  $\Gamma_{PA}$  values described previously.

Overall, our findings illuminate the intricate mechanisms underlying the multifaceted effects of arginine on hydrophobic

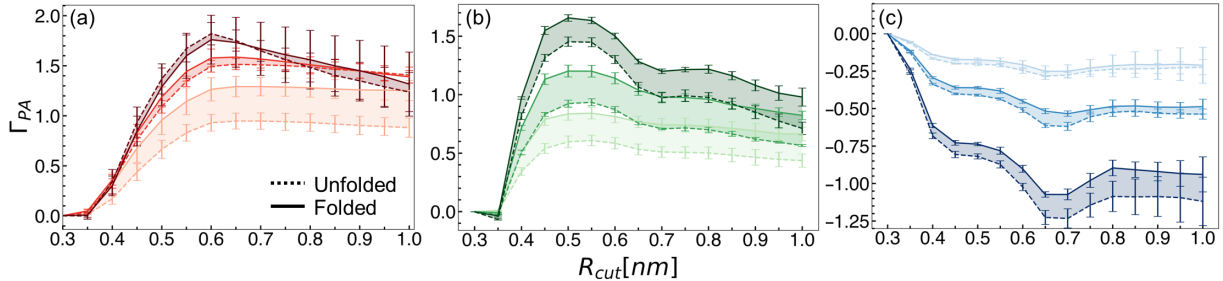


**Figure 4:** Preferential interaction coefficient values as a function of the cut-off distance for the local domain of the hydrophobic polymer for (a) arginine, (b) guanidinium, and (c) glycine. Dashed lines indicate values for the unfolded state, while solid lines denote the folded state. Increasing concentration is denoted by increased shading (light to dark). Mean values and errors were estimated from three replicate simulations. Errors are reported as standard deviations from mean values.

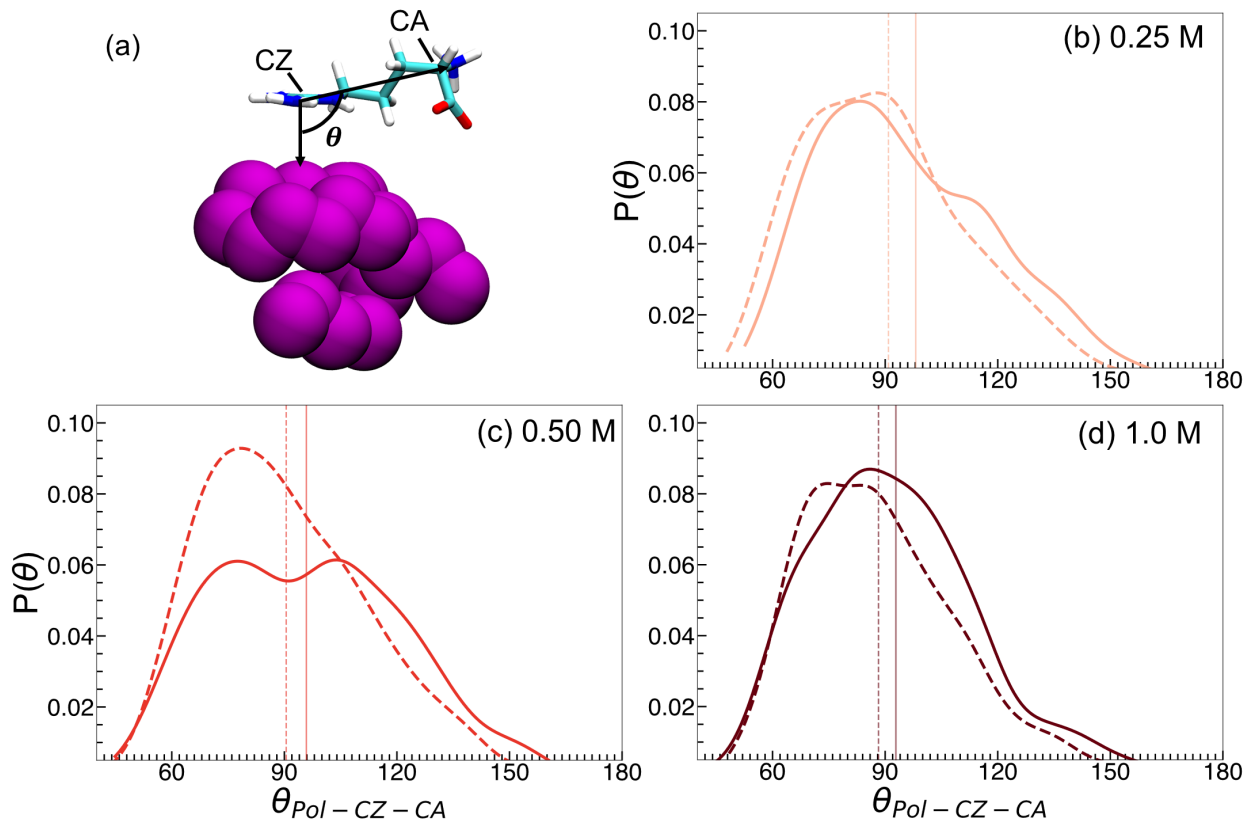


**Figure 5:** Preferential orientation of arginine relative to the hydrophobic polymer. (a) Representation of the three-body angle,  $\theta_{Pol-CZ-CA}$ .  $P(\theta)$  is shown for (b) 0.25 M, (c) 0.5 M, and (d) 1.0 M arginine concentrations. Solid lines denote the probability distribution for folded conformations, while dashed lines indicate the unfolded state. Vertical lines represent the ensemble average of each state.

polymer collapse. Arginine was observed to drophobic interactions, a key factor in pro-  
 increase the favorability of many-body hy- tein stabilization. Our observations reveal

a nuanced interplay in the impact of arginine on hydrophobic interactions, teetering on the edge of a mechanistic flip. At low concentrations, direct sidechain-driven interactions dominate, shifting to indirect backbone-driven effects at high concentrations.

The simultaneous presence of competing direct and indirect effects implies that changes in the chemistry of a protein surface, the addition of co-additives to solution, or differences in sample preparation may cause significant changes in the mechanism of action of arginine. A shift towards the direct mechanism risks denaturing native proteins by dis-

rupting electrostatic and hydrogen-bonding interactions. Conversely, a shift towards the indirect mechanism may yield stabilization of native proteins through preferential hydration. Our results suggest that arginine is uniquely situated for use in formulations due to its potential tunable, context-dependent properties. Hence, while arginine may not be considered the universal stabilizer it once was, its balance between direct- and indirect-driven stabilization of hydrophobic interactions solidifies its significance in formulation design.

## Acknowledgement

This material is based upon work supported by the National Science Foundation under DMREF Grant Nos. 2118788, 2118693, and 2118638.

## Supporting Information Available

Additional simulation details, error estimations, and figures are located in the Supporting Information.

## References

- (1) Jeong, S. H. Analytical methods and formulation factors to enhance protein stability in solution. *Arch. Pharm. Res.* **2012**, *35*, 1871–1886.
- (2) Wang, W. Protein aggregation and its inhibition in biopharmaceutics. *Int. J. Pharm.* **2005**, *289*, 1–30.

- (3) Patro, S. Y.; Freund, E.; Chang, B. S. Protein formulation and fill-finish operations. *Biotechnol. Annu. Rev.* **2002**, *8*, 55–84.
- (4) Arakawa, T.; Tsumoto, K.; Kita, Y.; Chang, B.; Ejima, D. Biotechnology applications of amino acids in protein purification and formulations. *Amino Acids* **2007**, *33*, 587–605.
- (5) Hamborsky, J.; Kroger, A.; Wolfe, C. *Epidemiology and prevention of vaccine-preventable diseases*, 13th ed.; Centers for Disease Control and Prevention: Atlanta, GA, 2015; OCLC: 915815516.
- (6) Mistilis, M. J.; Joyce, J. C.; Esser, E. S.; Skountzou, I.; Compans, R. W.; Bommaricus, A. S.; Prausnitz, M. R. Long-term stability of influenza vaccine in a dissolving microneedle patch. *Drug Deliv. and Transl. Res.* **2017**, *7*, 195–205.
- (7) Tsumoto, K.; Umetsu, M.; Kumagai, I.; Ejima, D.; Philo, J.; Arakawa, T. Role of Arginine in Protein Refolding, Solubilization, and Purification. *Biotechnol. Prog.* **2004**, *20*, 1301–1308.
- (8) Tsumoto, K.; Ejima, D.; Kita, Y.; Arakawa, T. Review: Why is arginine effective in suppressing aggregation? *Protein Pept. Lett.* **2005**, *12*, 613–619.
- (9) Stärtzel, P. Arginine as an Excipient for Protein Freeze-Drying: A Mini Review. *J. Pharm. Sci.* **2018**, *107*, 960–967.
- (10) Smirnova, E.; Safenkova, I.; Stein-Margolina, B.; Shubin, V.; Gurvits, B. l-Arginine induces protein aggregation and transformation of supramolecular structures of the aggregates. *Amino Acids* **2013**, *45*, 845–855.
- (11) Shah, D.; Shaikh, A. R.; Peng, X.; Rajagopalan, R. Effects of arginine on heat-induced aggregation of concentrated protein solutions. *Biotechnol. Prog.* **2011**, *27*, 513–520.

- (12) Eronina, T. B.; Chebotareva, N. A.; Sluchanko, N. N.; Mikhaylova, V. V.; Makeeva, V. F.; Roman, S. G.; Kleymenov, S. Y.; Kurganov, B. I. Dual effect of arginine on aggregation of phosphorylase kinase. *Int. J. Biol. Macromol.* **2014**, *68*, 225–232.
- (13) Xie, Q.; Guo, T.; Lu, J.; Zhou, H.-M. The guanidine like effects of arginine on aminocyclase and salt-induced molten globule state. *Int. J. Biochem. Cell Biol.* **2004**, *36*, 296–306.
- (14) Anumalla, B.; Prabhu, N. P. Counteracting Effect of Charged Amino Acids Against the Destabilization of Proteins by Arginine. *Appl. Biochem. Biotechnol.* **2019**, *189*, 541–555.
- (15) Arakawa, T.; Maluf, N. K. The effects of allantoin, arginine and NaCl on thermal melting and aggregation of ribonuclease, bovine serum albumin and lysozyme. *Int. J. Biol. Macromol.* **2018**, *107*, 1692–1696.
- (16) Meingast, C.; Heldt, C. L. Arginine-enveloped virus inactivation and potential mechanisms. *Biotechnol. Prog.* **2020**, *36*, e2931.
- (17) Vagenende, V.; Han, A. X.; Mueller, M.; Trout, B. L. Protein-Associated Cation Clusters in Aqueous Arginine Solutions and Their Effects on Protein Stability and Size. *ACS Chem. Biol.* **2013**, *8*, 416–422.
- (18) Platts, L.; Falconer, R. J. Controlling protein stability: Mechanisms revealed using formulations of arginine, glycine and guanidinium HCl with three globular proteins. *Int. J. Pharm.* **2015**, *486*, 131–135.
- (19) Arakawa, T.; Ejima, D.; Tsumoto, K.; Obeyama, N.; Tanaka, Y.; Kita, Y.; Timasheff, S. N. Suppression of protein interactions by arginine: a proposed mechanism of the arginine effects. *Biophys. Chem.* **2007**, *127*, 1–8.

- (20) Shukla, D.; Trout, B. L. Interaction of Arginine with Proteins and the Mechanism by Which It Inhibits Aggregation. *J. Phys. Chem. B* **2010**, *114*, 13426–13438.
- (21) Das, U.; Hariprasad, G.; Ethayathulla, A. S.; Manral, P.; Das, T. K.; Pasha, S.; Mann, A.; Ganguli, M.; Verma, A. K.; Bhat, R. et al. Inhibition of Protein Aggregation: Supramolecular Assemblies of Arginine Hold the Key. *PLoS ONE* **2007**, *2*, e1176.
- (22) Li, J.; Garg, M.; Shah, D.; Rajagopalan, R. Solubilization of aromatic and hydrophobic moieties by arginine in aqueous solutions. *J. Chem. Phys.* **2010**, *133*, 054902.
- (23) Schneider, C. P.; Trout, B. L. Investigation of Cosolute-Protein Preferential Interaction Coefficients: New Insight into the Mechanism by Which Arginine Inhibits Aggregation. *J. Phys. Chem. B* **2009**, *113*, 2050–2058.
- (24) Schneider, C. P.; Shukla, D.; Trout, B. L. Arginine and the Hofmeister Series: The Role of Ion–Ion Interactions in Protein Aggregation Suppression. *J. Phys. Chem. B* **2011**, *115*, 7447–7458.
- (25) Santra, S.; Dhurua, S.; Jana, M. Analyzing the driving forces of insulin stability in the basic amino acid solutions: A perspective from hydration dynamics. *J. Chem. Phys.* **2021**, *154*, 084901.
- (26) Santra, S.; Jana, M. Influence of Aqueous Arginine Solution on Regulating Conformational Stability and Hydration Properties of the Secondary Structural Segments of a Protein at Elevated Temperatures: A Molecular Dynamics Study. *J. Phys. Chem. B* **2022**, *126*, 1462–1476.
- (27) Kauzmann, W. Some Factors in the Interpretation of Protein Denaturation. *Adv. Prot. Chem.* **1959**, *14*, 1–63.

- (28) Tanford, C. Contribution of Hydrophobic Interactions to the Stability of the Globular Conformation of Proteins. *J. Am. Chem. Soc.* **1962**, *84*, 4240–4247.
- (29) Tanford, C. The Hydrophobic Effect and the Organization of Living Matter. *Science* **1978**, *200*, 1012–1018.
- (30) Dill, K. A. Dominant forces in protein folding. *Biochemistry* **1990**, *29*, 7133–7155.
- (31) Savage, H. J.; Elliott, C. J.; Freeman, C. M.; Finney, J. L. Lost hydrogen bonds and buried surface area: rationalising stability in globular proteins. *Faraday Trans.* **1993**, *89*, 2609–2617.
- (32) Hummer, G.; Garde, S.; Garcia, A.; Pratt, L. New perspectives on hydrophobic effects. *Chem. Phys.* **2000**, *258*, 349–370.
- (33) Pratt, L. R.; Pohorille, A. Hydrophobic Effects and Modeling of Biophysical Aqueous Solution Interfaces. *Chem. Rev.* **2002**, *102*, 2671–2692.
- (34) Ben-Naim, A. *Hydrophobic interactions*; Plenum Press: New York, 2005; OCLC: 911229893.
- (35) Chandler, D. Interfaces and the driving force of hydrophobic assembly. *Nature* **2005**, *437*, 640–647.
- (36) Timasheff, S. N. The Control of Protein Stability and Association by Weak Interactions with Water: How Do Solvents Affect These Processes? *Annu. Rev. Biophys. Biomol. Struct.* **1993**, *22*, 67–97.
- (37) Ghosh, T.; Kalra, A.; Garde, S. On the Salt-Induced Stabilization of Pair and Many-body Hydrophobic Interactions. *J. Phys. Chem. B* **2005**, *109*, 642–651.
- (38) Athawale, M. V.; Dordick, J. S.; Garde, S. Osmolyte Trimethylamine-N-Oxide Does Not Affect the Strength of Hydrophobic Interactions: Origin of Osmolyte Compatibility. *Biophys. J.* **2005**, *89*, 858–866.



- (39) Athawale, M. V.; Sarupria, S.; Garde, S. Enthalpy-Entropy Contributions to Salt and Osmolyte Effects on Molecular-Scale Hydrophobic Hydration and Interactions. *J. Phys. Chem. B* **2008**, *112*, 5661–5670.
- (40) Zangi, R.; Zhou, R.; Berne, B. J. Urea’s Action on Hydrophobic Interactions. *J. Am. Chem. Soc.* **2009**, *131*, 1535–1541.
- (41) Canchi, D. R.; Garcia, A. E. Cosolvent Effects on Protein Stability. *Annu. Rev. Phys. Chem.* **2013**, *64*, 273–293.
- (42) van der Vegt, N. F. A.; Nayar, D. The Hydrophobic Effect and the Role of Cosolvents. *J. Phys. Chem. B* **2017**, *121*, 9986–9998.
- (43) Paul, S.; Patey, G. N. Hydrophobic Interactions in Urea-Trimethylamine-*N*-oxide Solutions. *J. Phys. Chem. B* **2008**, *112*, 11106–11111.
- (44) Macdonald, R. D.; Khajepour, M. Effects of the osmolyte TMAO (Trimethylamine-*N*-oxide) on aqueous hydrophobic contact-pair interactions. *Biophys. Chem.* **2013**, *184*, 101–107.
- (45) Ganguly, P.; Van Der Vegt, N. F. A.; Shea, J.-E. Hydrophobic Association in Mixed Urea-TMAO Solutions. *J. Phys. Chem. Lett.* **2016**, *7*, 3052–3059.
- (46) Su, Z.; Ravindhran, G.; Dias, C. L. Effects of Trimethylamine- *N* -oxide (TMAO) on Hydrophobic and Charged Interactions. *J. Phys. Chem. B* **2018**, *122*, 5557–5566.
- (47) Folberth, A.; Bharadwaj, S.; Van Der Vegt, N. F. A. Small-to-large length scale transition of TMAO interaction with hydrophobic solutes. *Phys. Chem. Chem. Phys.* **2022**, *24*, 2080–2087.
- (48) Wallqvist, A.; Covell, D. G.; Thirumalai, D. Hydrophobic Interactions in Aqueous Urea Solutions with Implications for the Mechanism of Protein Denaturation. *J. Am. Chem. Soc.* **1998**, *120*, 427–428.

- (49) Ikeguchi, M.; Nakamura, S.; Shimizu, K. Molecular Dynamics Study on Hydrophobic Effects in Aqueous Urea Solutions. *J. Am. Chem. Soc.* **2001**, *123*, 677–682.
- (50) Van Der Vegt, N. F. A.; Lee, M.-E.; Trzesniak, D.; Van Gunsteren, W. F. Enthalpy-Entropy Compensation in the Effects of Urea on Hydrophobic Interactions. *J. Phys. Chem. B* **2006**, *110*, 12852–12855.
- (51) Lee, M.-E.; Van Der Vegt, N. F. A. Does Urea Denature Hydrophobic Interactions? *J. Am. Chem. Soc.* **2006**, *128*, 4948–4949.
- (52) Shpiruk, T. A.; Khajepour, M. The effect of urea on aqueous hydrophobic contact-pair interactions. *Phys. Chem. Chem. Phys.* **2013**, *15*, 213–222.
- (53) Wang, A.; Bolen, D. W. A Naturally Occurring Protective System in Urea-Rich Cells: Mechanism of Osmolyte Protection of Proteins against Urea Denaturation. *Biochemistry* **1997**, *36*, 9101–9108.
- (54) Zou, Q.; Bennion, B. J.; Daggett, V.; Murphy, K. P. The Molecular Mechanism of Stabilization of Proteins by TMAO and Its Ability to Counteract the Effects of Urea. *J. Am. Chem. Soc.* **2002**, *124*, 1192–1202.
- (55) Bennion, B. J.; Daggett, V. The molecular basis for the chemical denaturation of proteins by urea. *Proc. Natl. Acad. Sci. U.S.A.* **2003**, *100*, 5142–5147.
- (56) ten Wolde, P. R.; Chandler, D. Drying-induced hydrophobic polymer collapse. *Proc. Natl. Acad. Sci. U.S.A.* **2002**, *99*, 6539–6543.
- (57) Nayar, D.; van der Vegt, N. F. A. Cosolvent Effects on Polymer Hydration Drive Hydrophobic Collapse. *J. Phys. Chem. B* **2018**, *122*, 3587–3595.
- (58) Mondal, J.; Stirnemann, G.; Berne, B. J. When Does Trimethylamine *N*-Oxide Fold a Polymer Chain and Urea Unfold It? *J. Phys. Chem. B* **2013**, *117*, 8723–8732.

- (59) Jamadagni, S. N.; Godawat, R.; Garde, S. How Surface Wettability Affects the Binding, Folding, and Dynamics of Hydrophobic Polymers at Interfaces. *Langmuir* **2009**, *25*, 13092–13099.
- (60) Sugita, Y.; Kitao, A.; Okamoto, Y. Multidimensional replica-exchange method for free-energy calculations. *J. Chem. Phys.* **2000**, *113*, 6042–6051.
- (61) Van Der Spoel, D.; Lindahl, E.; Hess, B.; Groenhof, G.; Mark, A. E.; Berendsen, H. J. C. GROMACS: Fast, flexible, and free. *J. Comput. Chem.* **2005**, *26*, 1701–1718.
- (62) Abraham, M. J.; Murtola, T.; Schulz, R.; Páll, S.; Smith, J. C.; Hess, B.; Lindahl, E. GROMACS: High performance molecular simulations through multi-level parallelism from laptops to supercomputers. *SoftwareX* **2015**, *1-2*, 19–25.
- (63) Bonomi, M.; Branduardi, D.; Bussi, G.; Camilloni, C.; Provasi, D.; Raiteri, P.; Donadio, D.; Marinelli, F.; Pietrucci, F.; Broglia, R. A. et al. PLUMED: A portable plugin for free-energy calculations with molecular dynamics. *Comput. Phys. Commun.* **2009**, *180*, 1961–1972.
- (64) Tribello, G. A.; Bonomi, M.; Branduardi, D.; Camilloni, C.; Bussi, G. PLUMED 2: New feathers for an old bird. *Comp. Phys. Comm.* **2014**, *185*, 604–613.
- (65) Abascal, J. L. F.; Vega, C. A general purpose model for the condensed phases of water: TIP4P/2005. *J. Chem. Phys.* **2005**, *123*, 234505.
- (66) Brooks, B. R.; Brooks, C. L.; Mackerell, A. D.; Nilsson, L.; Petrella, R. J.; Roux, B.; Won, Y.; Archontis, G.; Bartels, C.; Boresch, S. et al. CHARMM: The biomolecular simulation program. *J. Comput. Chem.* **2009**, *30*, 1545–1614.
- (67) Lorentz, H. A. Ueber die Anwendung des Satzes vom Virial in der kinetischen Theorie der Gase. *Annalen der Physik* **1881**, *248*, 127–136.

- (68) Zhu, F.; Hummer, G. Convergence and error estimation in free energy calculations using the weighted histogram analysis method. *J Comput. Chem.* **2012**, *33*, 453–465.
- (69) Athawale, M. V.; Goel, G.; Ghosh, T.; Truskett, T. M.; Garde, S. Effects of length-scales and attractions on the collapse of hydrophobic polymers in water. *Proc. Natl. Acad. Sci. U.S.A.* **2007**, *104*, 733–738.
- (70) Godawat, R.; Jamadagni, S. N.; Garde, S. Unfolding of Hydrophobic Polymers in Guanidinium Chloride Solutions. *J. Phys. Chem. B* **2010**, *114*, 2246–2254.
- (71) Dasetty, S.; Sarupria, S. Advancing Rational Control of Peptide–Surface Complexes. *J. Phys. Chem. B* **2021**, *125*, 2644–2657.
- (72) Stillinger, F. H. Structure in aqueous solutions of nonpolar solutes from the standpoint of scaled-particle theory. *J. Solution Chem.* **1973**, *2*, 141–158.
- (73) Lum, K.; Chandler, D.; Weeks, J. D. Hydrophobicity at Small and Large Length Scales. *J. Phys. Chem. B* **1999**, *103*, 4570–4577.
- (74) Goel, G.; Athawale, M. V.; Garde, S.; Truskett, T. M. Attractions, Water Structure, and Thermodynamics of Hydrophobic Polymer Collapse. *J. Phys. Chem. B* **2008**, *112*, 13193–13196.
- (75) Makowski, M.; Czaplewski, C.; Liwo, A.; Scheraga, H. A. Potential of Mean Force of Association of Large Hydrophobic Particles: Toward the Nanoscale Limit. *J. Phys. Chem. B* **2010**, *114*, 993–1003.
- (76) Ben-Amotz, D. Water-Mediated Hydrophobic Interactions. *Annu. Rev. Phys. Chem.* **2016**, *67*, 617–638.
- (77) Dhabal, D.; Jiang, Z.; Pallath, A.; Patel, A. J. Characterizing the Interplay between Polymer Solvation and Conformation. *J. Phys. Chem. B* **2021**, *125*, 5434–5442.

- (78) Kalra, A.; Tugcu, N.; Cramer, S. M.; Garde, S. Salting-In and Salting-Out of Hydrophobic Solutes in Aqueous Salt Solutions. *J. Phys. Chem. B* **2001**, *105*, 6380–6386.
- (79) Lin, T.-Y.; Timasheff, S. N. On the role of surface tension in the stabilization of globular proteins: Stabilization of globular proteins. *Prot. Sci.* **1996**, *5*, 372–381.
- (80) Kita, Y.; Arakawa, T.; Lin, T.-Y.; Timasheff, S. N. Contribution of the Surface Free Energy Perturbation to Protein-Solvent Interactions. *Biochemistry* **1994**, *33*, 15178–15189.
- (81) Arakawa, T.; Timasheff, S. The stabilization of proteins by osmolytes. *Biophys. J.* **1985**, *47*, 411–414.
- (82) Bauer, K. C.; Suhm, S.; Wöll, A. K.; Hubbuch, J. Impact of additives on the formation of protein aggregates and viscosity in concentrated protein solutions. *Int. J. Pharm.* **2017**, *516*, 82–90.
- (83) Watlafer, D. B.; Malik, S. K.; Stoller, L.; Coffin, R. L. Nonpolar Group Participation in the Denaturation of Proteins by Urea and Guanidinium Salts. Model Compound Studies. *J. Am. Chem. Soc.* **1964**, *86*, 508–514.
- (84) Meuzelaar, H.; Panman, M. R.; Woutersen, S. Guanidinium-Induced Denaturation by Breaking of Salt Bridges. *Angew. Chem.* **2015**, *127*, 15470–15474.
- (85) Jha, S. K.; Marqusee, S. Kinetic evidence for a two-stage mechanism of protein denaturation by guanidinium chloride. *Proc. Natl. Acad. Sci. U.S.A.* **2014**, *111*, 4856–4861.
- (86) Dempsey, C. E.; Mason, P. E.; Brady, J. W.; Neilson, G. W. The Reversal by Sulfate of the Denaturant Activity of Guanidinium. *J. Am. Chem. Soc.* **2007**, *129*, 15895–15902.
- (87) Heyda, J.; Okur, H. I.; Hladílková, J.; Rembert, K. B.; Hunn, W.; Yang, T.; Dzubella, J.; Jungwirth, P.; Cremer, P. S. Guanidinium can both Cause and Prevent the Hydrophobic Collapse of Biomacromolecules. *J. Am. Chem. Soc.* **2017**, *139*, 863–870.

- (88) Ferrario, M.; Haughney, M.; McDonald, I. R.; Klein, M. L. Molecular-dynamics simulation of aqueous mixtures: Methanol, acetone, and ammonia. *J. Chem. Phys.* **1990**, *93*, 5156–5166.
- (89) Luzar, A.; Chandler, D. Structure and hydrogen bond dynamics of water–dimethyl sulfoxide mixtures by computer simulations. *J. Chem. Phys.* **1993**, *98*, 8160–8173.
- (90) Luzar, A.; Chandler, D. Hydrogen-bond kinetics in liquid water. *Nature* **1996**, *379*, 55–57.
- (91) Luzar, A. Resolving the hydrogen bond dynamics conundrum. *J. Chem. Phys.* **2000**, *113*, 10663–10675.
- (92) Vazdar, M.; Heyda, J.; Mason, P. E.; Tesei, G.; Allolio, C.; Lund, M.; Jungwirth, P. Arginine “Magic”: Guanidinium Like-Charge Ion Pairing from Aqueous Salts to Cell Penetrating Peptides. *Acc. Chem. Res.* **2018**, *51*, 1455–1464.
- (93) Gund, P. Guanidine, trimethylenemethane, and “Y-delocalization.” Can acyclic compounds have “aromatic” stability? *J. Chem. Educ.* **1972**, *49*, 100.
- (94) Scatchard, G. Physical Chemistry of Protein Solutions. I. Derivation of the Equations for the Osmotic Pressure <sup>1</sup>. *J. Am. Chem. Soc.* **1946**, *68*, 2315–2319.
- (95) Casassa, E. F.; Eisenberg, H. *Adv. Prot. Chem.*; Elsevier, 1964; Vol. 19; pp 287–395.
- (96) Schellman, J. A. Selective binding and solvent denaturation. *Biopolymers* **1987**, *26*, 549–559.
- (97) Inoue, H.; Timasheff, S. N. Preferential and absolute interactions of solvent components with proteins in mixed solvent systems. *Biopolymers* **1972**, *11*, 737–743.
- (98) Record, M.; Anderson, C. Interpretation of preferential interaction coefficients of non-electrolytes and of electrolyte ions in terms of a two-domain model. *Biophys. J.* **1995**, *68*, 786–794.

- (99) Shukla, D.; Shinde, C.; Trout, B. L. Molecular Computations of Preferential Interaction Coefficients of Proteins. *J. Phys. Chem. B* **2009**, *113*, 12546–12554.
- (100) Wyman, J. *Adv. Protein Chem.*; Elsevier, 1964; Vol. 19; pp 223–286.
- (101) Timasheff, S. N. Protein-solvent preferential interactions, protein hydration, and the modulation of biochemical reactions by solvent components. *Proc. Natl. Acad. Sci. U.S.A.* **2002**, *99*, 9721–9726.
- (102) Shukla, D.; Schneider, C. P.; Trout, B. L. Molecular level insight into intra-solvent interaction effects on protein stability and aggregation. *Adv. Drug Delivery Rev.* **2011**, *63*, 1074–1085.
- (103) Mondal, J.; Halverson, D.; Li, I. T. S.; Stirnemann, G.; Walker, G. C.; Berne, B. J. How osmolytes influence hydrophobic polymer conformations: A unified view from experiment and theory. *Proc. Natl. Acad. Sci. U.S.A.* **2015**, *112*, 9270–9275.
- (104) Mukherjee, M.; Mondal, J. Unifying the Contrasting Mechanisms of Protein-Stabilizing Osmolytes. *J. Phys. Chem. B* **2020**, *124*, 6565–6574.
- (105) Shukla, D.; Trout, B. L. Preferential Interaction Coefficients of Proteins in Aqueous Arginine Solutions and Their Molecular Origins. *J. Phys. Chem. B* **2011**, *115*, 1243–1253.

# Supplementary Information

## Flipping Out: Role of Arginine in Hydrophobic Polymer Collapse

Jonathan W. P. Zajac,<sup>†</sup> Praveen Muralikrishnan,<sup>‡</sup> Caryn L. Heldt,<sup>¶</sup> Sarah L.  
Perry,<sup>§</sup> and Sapna Sarupria<sup>\*,†</sup>

<sup>†</sup>*Department of Chemistry, University of Minnesota, Minneapolis, MN 55455, USA*

<sup>‡</sup>*Department of Chemical Engineering and Materials Science, University of Minnesota,  
Minneapolis, MN 55455, USA*

<sup>¶</sup>*Department of Chemical Engineering, Michigan Technological University, Houghton, MI  
49931, USA*

<sup>§</sup>*Department of Chemical Engineering, University of Massachusetts Amherst, MA 01003,  
USA*

<sup>||</sup>*Chemical Theory Center, University of Minnesota, Minneapolis, MN 55455, USA*

E-mail: sarupria@umn.edu



# Simulation Details

A cubic box of length of 6.74 nm was constructed with a padding of 1.5 nm between the edge of the fully extended polymer and the nearest box edge. Chloride ( $\text{Cl}^-$ ) counterions equal to the number of arginine molecules were added to achieve a net charge of zero. The TIP4P/2005<sup>1</sup> model was used for water, and the CHARMM22 force field was used for arginine and  $\text{Cl}^-$ .<sup>2</sup> Lorentz-Berthelot mixing rules<sup>3</sup> were used to calculate non-bonded interactions between different atom types, except polymer-water oxygen interactions (Table S1). Polymer-water oxygen interactions were adjusted iteratively until the folded and unfolded states of the polymer were approximately evenly distributed in straightforward MD simulations. The various Lennard-Jones parameters tested are presented in Table S1. Guided by radius of gyration ( $R_g$ ) probability distributions, we selected parameters of model 2 for our study (Figure S2).

**Table S1: Polymer interaction parameters used in the present study.**

Interaction	Model	Sigma (nm)	Epsilon (kJ/mol)
Polymer-Polymer	All	0.373	0.586
Polymer-Water	Model 1	0.345	0.573
Polymer-Water	Model 2	0.345	0.593
Polymer-Water	Model 3	0.345	0.620
Polymer-Water	Model 4	0.345	0.674

REUS simulations were performed in 12 evenly-spaced windows along the  $R_g$  reaction coordinate, spanning 0.35 nm to 0.9 nm. Each window was biased according to a harmonic potential, with a force constant of 1000 kJ/mol/nm<sup>2</sup> for the window centered at 0.45 nm (window 3) and 5000 kJ/mol/nm<sup>2</sup> for all other windows. We observed inefficient sampling in window 3 region (Fig. S3). Subsequent simulations with varying force constants for window 3 regions revealed that a force constant of 1000 kJ/mol/nm<sup>2</sup> minimized differences between replicate runs in the regions close to the window centers.

The windows are first energy minimized using the steepest descent minimization with a tolerance of 10 kJ/mol/nm and step size of 0.01. For each window, 1 ns NVT equilibration

is then performed using V-rescale thermostat (temperature coupling time constant,  $\tau_T = 0.5$  ps),<sup>4</sup> followed by 1 ns NPT equilibration using the V-rescale thermostat ( $\tau_T = 0.5$  ps)<sup>4</sup> and Berendsen barostat ( $\tau_P = 0.5$  ps)<sup>5</sup> to bring the system to a temperature of 300 K and pressure of 1 atm. NPT production run for 100 ns is simulated for each window using Nosé-Hoover temperature coupling ( $\tau_T = 5$  ps)<sup>6</sup> and Parrinello-Rahman pressure coupling ( $\tau_P = 25$  ps).<sup>7</sup> A Hamiltonian exchange move is attempted every 200 timesteps, with a 2 fs time step. The Particle Mesh Ewald (PME) algorithm was used for electrostatic interactions with a cut-off of 1 nm. A reciprocal grid of 42 x 42 x 42 cells was used with 4<sup>th</sup> order B-spline interpolation. A single cut-off of 1 nm was used for Van der Waals interactions. The neighbor search was performed every 10 steps.

To further investigate the hypothesis that attractive polymer-arginine interactions are driven by the guanidinium sidechain while indirect effects are driven by the backbone, additional independent REUS simulations including either guanidinium or glycine as the additive were carried out. Guanidinium parameters were based on the CHARMM22 parameters of arginine. This was achieved by truncating an arginine molecule up to the first guanidinium nitrogen, protonating this atom, and imposing a symmetric charge distribution according to the existing parameters. Glycine parameters were taken directly from the CHARMM22 force field. Systems in the same concentration range as arginine were generated to study sidechain and backbone contributions to hydrophobic polymer collapse.

## Error Calculations

The errors for PMF were calculated through the propagation of uncertainty using 3 replicate simulations ( $N = 3$ ). The derivation of uncertainty in the free energy of unfolding is shown below.  $\sigma$  represents the standard deviation, exp represents the exponential term, ln represents the logarithmic term and int represents the integral.

**Table S2: Setup of simulated systems.**

System	Simulation Time (ns)	Concentration (M)	$N_{Exc}$	$N_{Wat}$
Arginine	20	0.25	47	9653
Arginine	20	0.50	93	9111
Arginine	20	0.75	139	8582
Arginine	20	1.0	185	7933
Polymer	100 x 12	0.00	0	10599
Polymer + Arginine	100 x 12	0.25	47	10092
Polymer + Arginine	100 x 12	0.50	93	9511
Polymer + Arginine	250 x 12	1.0	185	8398
Polymer + Guanidinium	50 x 12	0.25	47	10364
Polymer + Guanidinium	50 x 12	0.50	93	10144
Polymer + Guanidinium	50 x 12	1.0	185	9702
Polymer + Glycine	50 x 12	0.25	47	10318
Polymer + Glycine	50 x 12	0.50	93	10022
Polymer + Glycine	50 x 12	1.0	185	9444

$$\Delta G_{\text{unfold}} = k_B T \ln \frac{\int_{R_g^{\text{cut}}}^{R_g^{\text{max}}} \exp\left(-\frac{W(R_g)}{k_B T}\right) dR_g}{\int_{R_g^{\text{min}}}^{R_g^{\text{cut}}} \exp\left(-\frac{W(R_g)}{k_B T}\right) dR_g} \quad (1)$$

The integral is approximated as a sum and divided into discrete bins in the  $R_g$  coordinate.

The  $R_g$  space (from 0.3 to 0.9 nm) is divided into 600 bins, giving a  $\Delta R_g = 0.001$  nm.

$$\sigma_{W(R_g)} = \sqrt{\frac{\sum (W(R_g)_i - \mu_{W(R_g)})^2}{N}} \quad (2)$$

$$\sigma_{\text{exp}} = \left| \exp\left(-\frac{W(R_g)}{k_B T}\right) \right| * \left| \frac{1}{k_B T} * \sigma_{W(R_g)} \right| \quad (3)$$

$$\sigma_{\text{int}} = \Delta R_g * \sqrt{\sum \sigma_{\text{exp}}^2} \quad (4)$$

$$\sigma_{ln} = \frac{\sigma_{\text{int}}}{\text{int}} \quad (5)$$

$$\sigma_{\Delta G} = k_B T * \sqrt{(\sigma_{ln})_{num}^2 + (\sigma_{ln})_{den}^2} \quad (6)$$

The errors in PMF decomposition were calculated using error propagation rules. An example of error calculation for  $\Delta E_{unfold}$  is shown below:

$$\Delta E_{unfold} = \langle E \rangle_u - \langle E \rangle_f \quad (7)$$

$$\langle E \rangle_f = \frac{\sum_{r_{min}}^{r_{cut}} E(R_g) P(R_g)}{\sum_{r_{min}}^{r_{cut}} P(R_g)}, \quad \langle E \rangle_u = \frac{\sum_{r_{cut}}^{r_{max}} E(R_g) P(R_g)}{\sum_{r_{cut}}^{r_{max}} P(R_g)} \quad (8)$$

$$\sigma_{E(R_g)} = \sqrt{\frac{\sum (E(R_g)_i - \mu_{E(R_g)})^2}{N}} \quad (9)$$

$$\sigma_{\langle E \rangle} = \frac{\sqrt{\sum_{r_{min}}^{r_{cut}} \sigma_{E(R_g)}^2 P(R_g)^2}}{\sum_{r_{min}}^{r_{cut}} P(R_g)} \quad (10)$$

$$\sigma_{\Delta E} = \sqrt{\sigma_{int,f}^2 + \sigma_{int,u}^2} \quad (11)$$

## Clustering Analyses

Clustering was achieved via the leaf algorithm of HDBSCAN.<sup>8</sup> The minimum cluster size parameter was set to 100, while the minimum samples parameter was set to 50. Clustering was carried out on the principal moments of the gyration tensor of the hydrophobic polymer. Data were obtained from the final 100 ns in each window (3.6  $\mu$ s total), saving coordinates every 100 ps. Data points not belonging to clusters were removed, for clarity. Clusters identified in principal moment space were projected onto end-to-end vs radius of gyration space. Representative snapshots are shown in Fig S5 to illustrate the configurations obtained in each cluster. Clusters at  $R_g = 0.4$  and  $R_g = 0.5$  are separated by a free energy barrier in

the calculated PMFs.

## Preferential Interaction Coefficients

In the main text, we denote water, polymer, and additive as W, P, and A, respectively. Here, we follow traditional notation found in literature, denoting water, polymer, and additive as 1, 2, and 3, respectively. At higher concentrations, no preference for folded versus unfolded conformations was observed.  $\text{Cl}^-$  was found to preferentially deplete from the local domain of the polymer at both high and low concentrations (Fig. S11), as expected. For a binary electrolyte such as ArgCl, the net preferential interaction coefficient is obtained as<sup>9</sup>

$$\Gamma_{23} = 0.5(\Gamma_{23}^- + \Gamma_{23}^+ - |Z|) \tag{12}$$

where  $\Gamma_{23,-}$  denotes the preferential interaction coefficient for the anion,  $\Gamma_{23,+}$  for the cation, and  $Z$  is the charge of the solute (for the polymer,  $Z = 0$ ).

The net preferential interaction coefficient of the binary electrolyte ArgCl is reported in Fig. S11. The observed increase in  $\Gamma_{23}^{\text{ArgCl}}$  with increasing concentration is in contrast to experimental evidence suggesting arginine tends to preferentially interact with proteins at low concentrations and becomes excluded with increasing concentration.<sup>10-13</sup> Our findings suggest that this concentration-dependent behavior of arginine is likely not mediated by the presence of hydrophobic interaction sites.

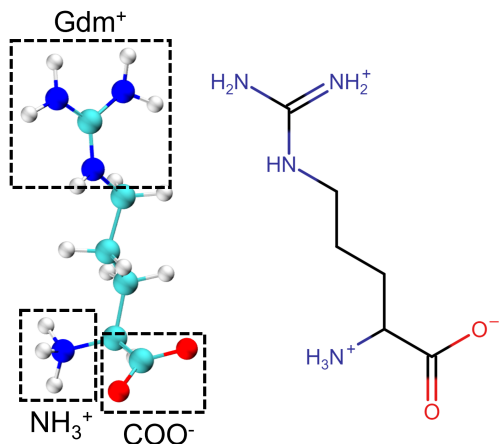


Figure S1: Representation of the structure of arginine. Boxes are drawn around the charged groups of arginine.

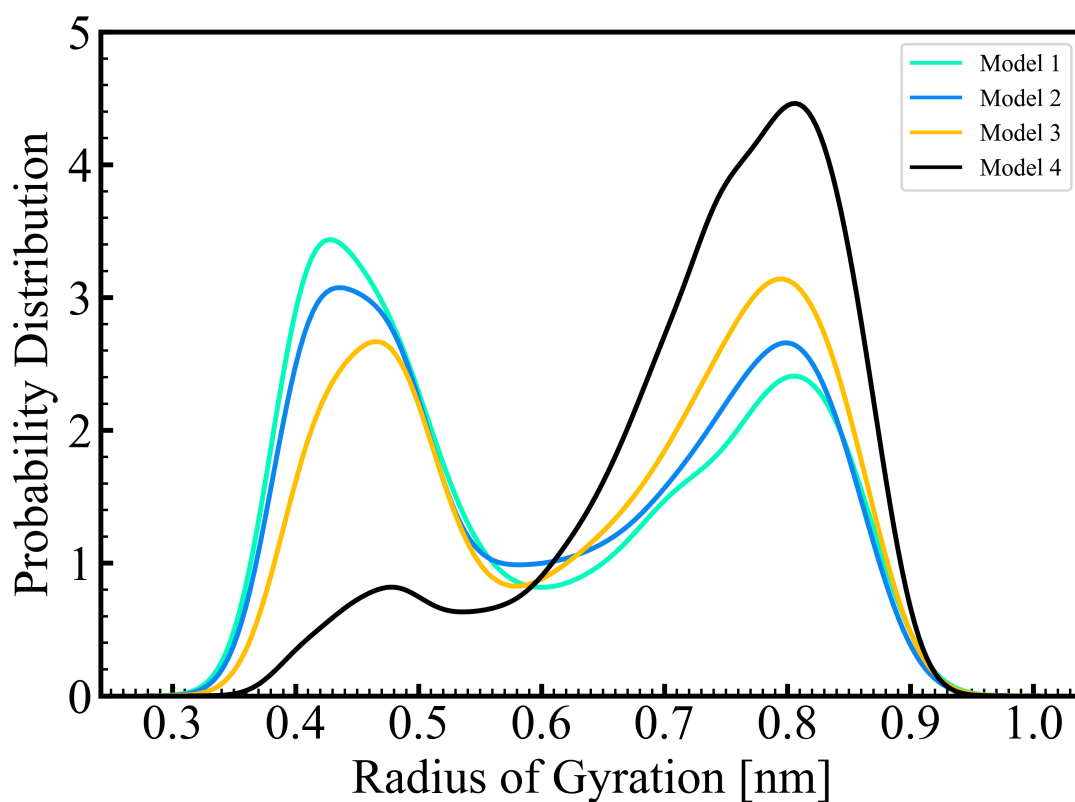


Figure S2: Probability Distribution of radius of gyration obtained from 50 ns simulations of different polymer models in pure water. The models differ in their polymer-water interaction parameter,  $\epsilon$ , having 85% (model 1), 88% (model 2), 92% (model 3), and 100% (model 4) of the value calculated from Lorentz-Berthelot mixing rules.

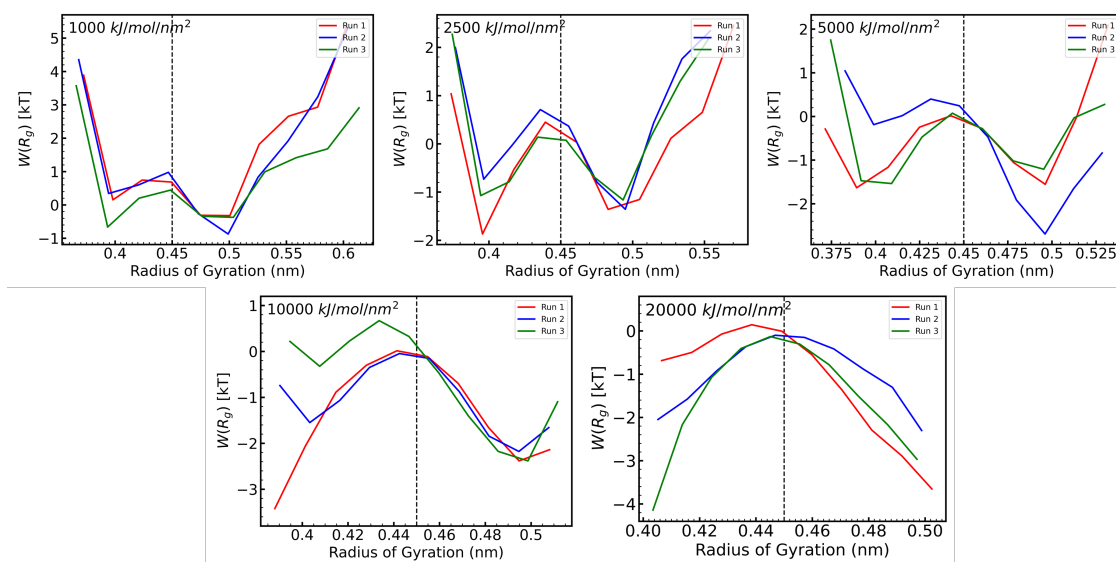


Figure S3: Sampling of 3 replicate runs in the window 3 (reference radius of gyration = 0.45 nm) region for polymer in 0.75M arginine solution with different force constants ranging from 1000 - 20000  $kJ/mol/nm^2$ . For regions close to the reference, the uncertainty between runs is lesser for the lower force constant values. Force constant 1000  $kJ/mol/nm^2$  was chosen for window 3 based on these observations

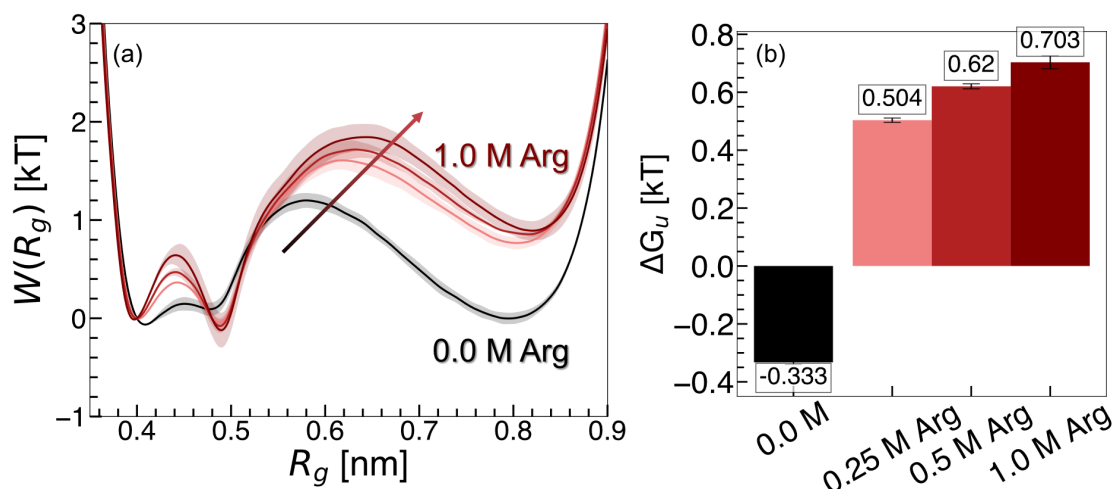


Figure S4: PMFs and free energies of unfolding obtained from REUS simulations. (a) PMFs of hydrophobic polymer along  $R_g$  in pure water (black) and arginine (red) solutions. The arrow indicates the direction of increasing arginine concentration. All plots are normalized to 0 at  $R_g = 0.4$  nm. (b) Free energies of hydrophobic polymer unfolding ( $\Delta G_u$ ). Error bars were estimated as the standard deviation of PMFs obtained from three replicate simulations.

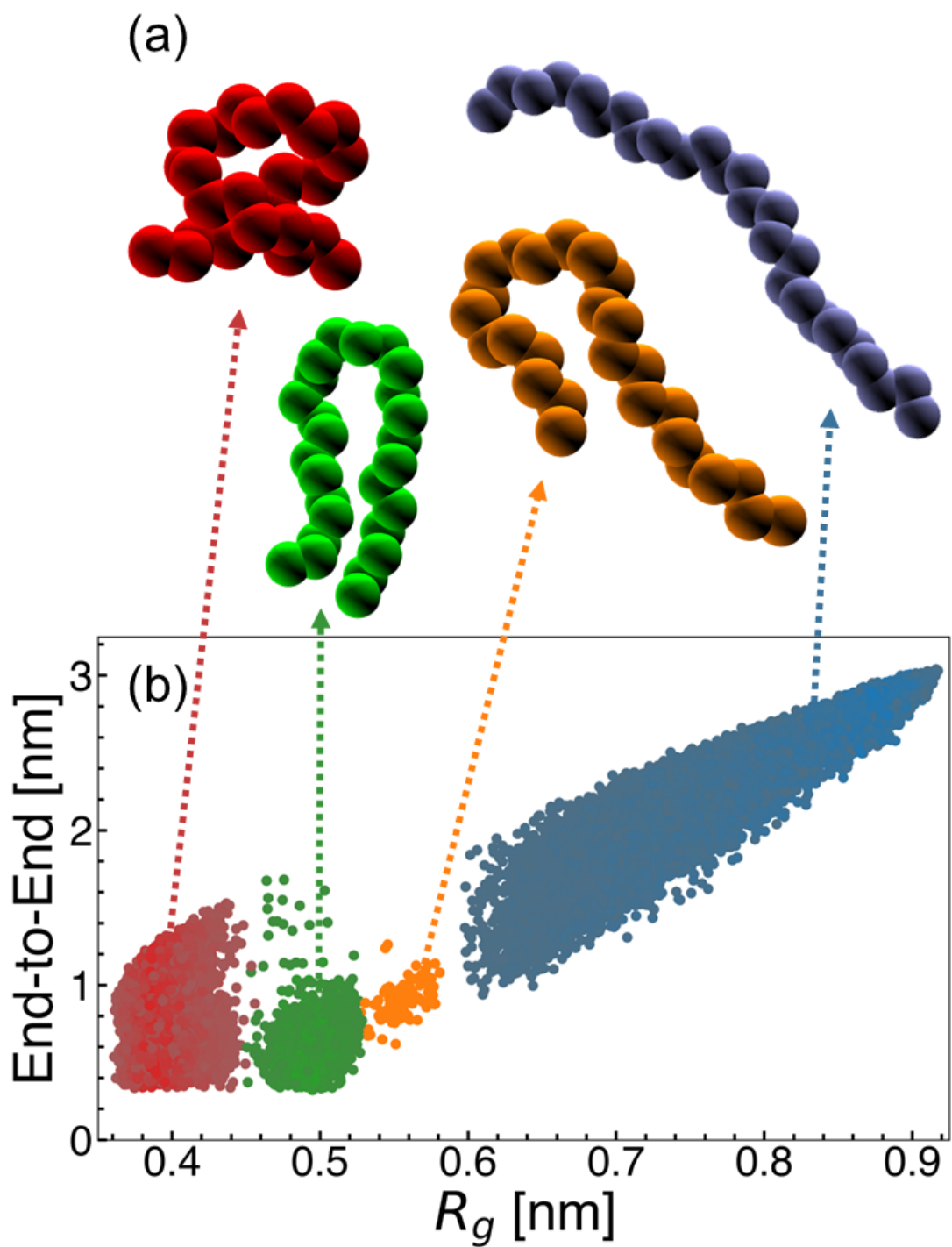


Figure S5: (a) Representative configurations from HDBSCAN clustering in 0.25 M arginine solution. (b) Polymer configurations projected onto end-to-end distance and radius of gyration space.



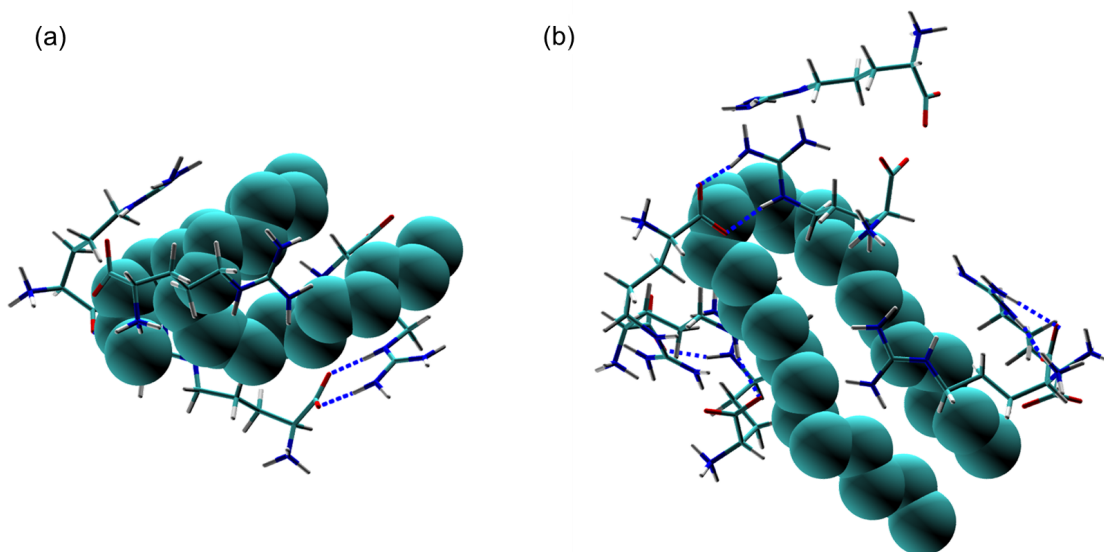


Figure S6: Representative snapshots of arginine encapsulating structures observed at the hydrophobic polymer surface. Snapshots extracted from the hydrophobic polymer in (a) unfolded and (b) folded REUS windows.

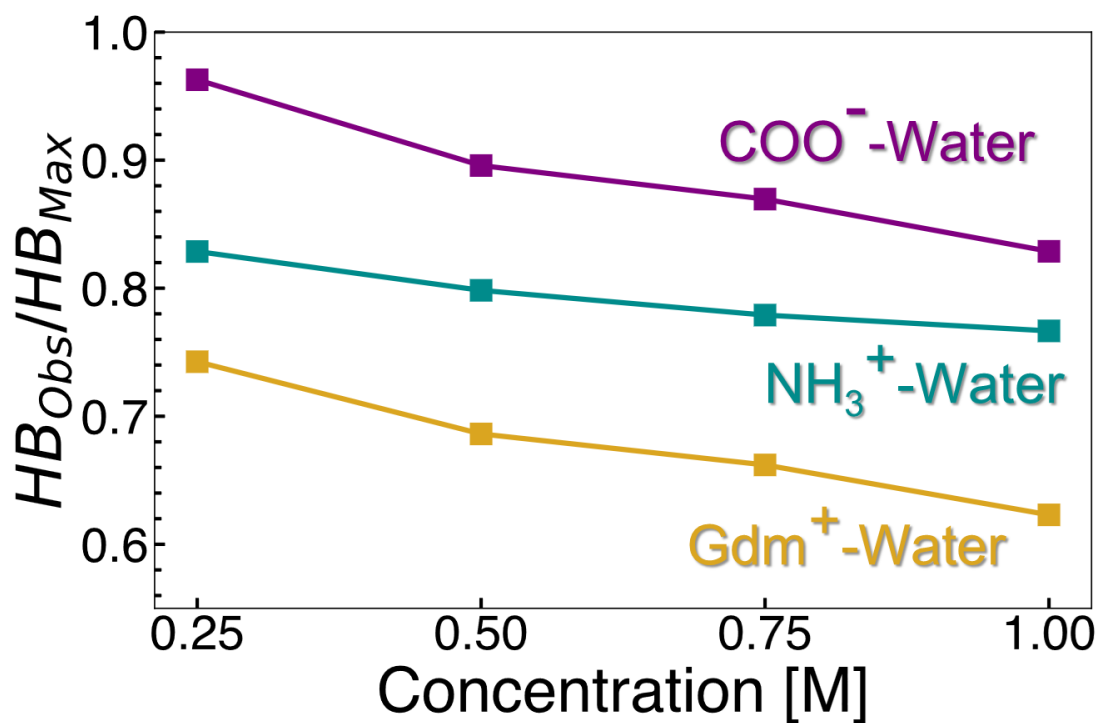


Figure S7: Fraction of observed hydrogen bonds ( $HB_{Obs}$ ) relative to maximum number of hydrogen bonds ( $HB_{Max}$ ) per interaction group.

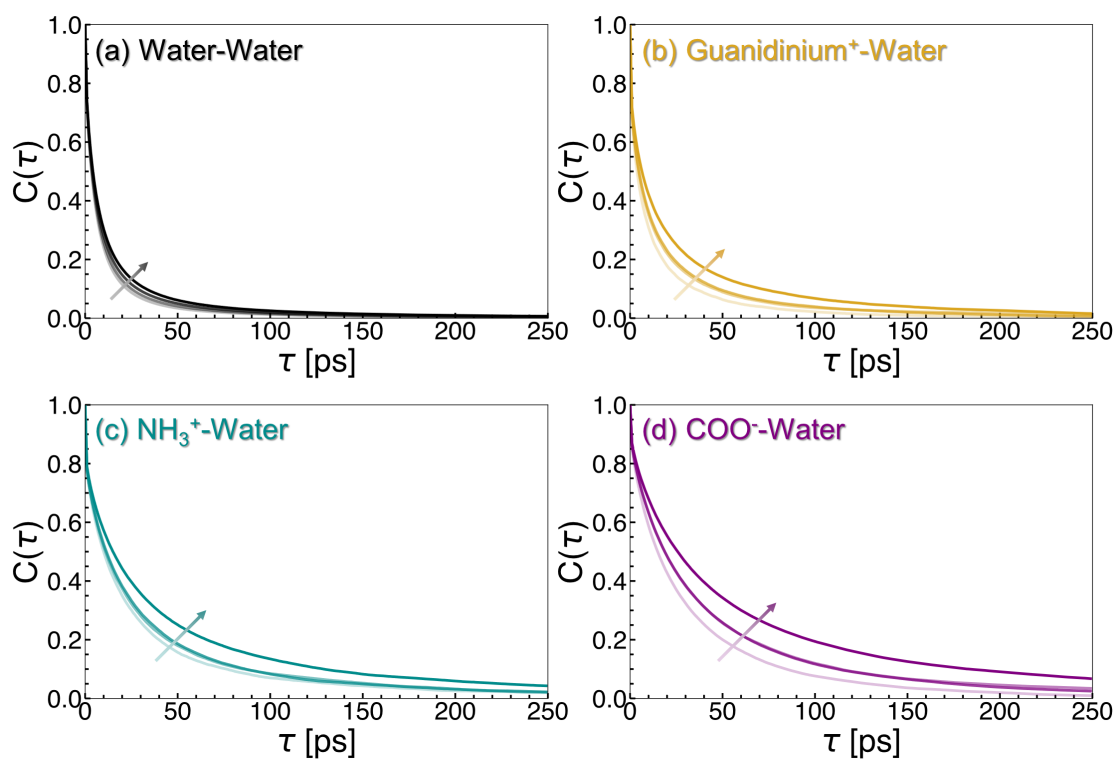


Figure S8: Hydrogen bond existence correlation functions for (a) water-water, (b) guanidinium<sup>+</sup>-water, (c) NH<sub>3</sub><sup>+</sup>-water, and (d) COO<sup>-</sup>-water. Each plot is shown as a function of concentration, with increased shading (light to dark) denoting increasing arginine concentration.

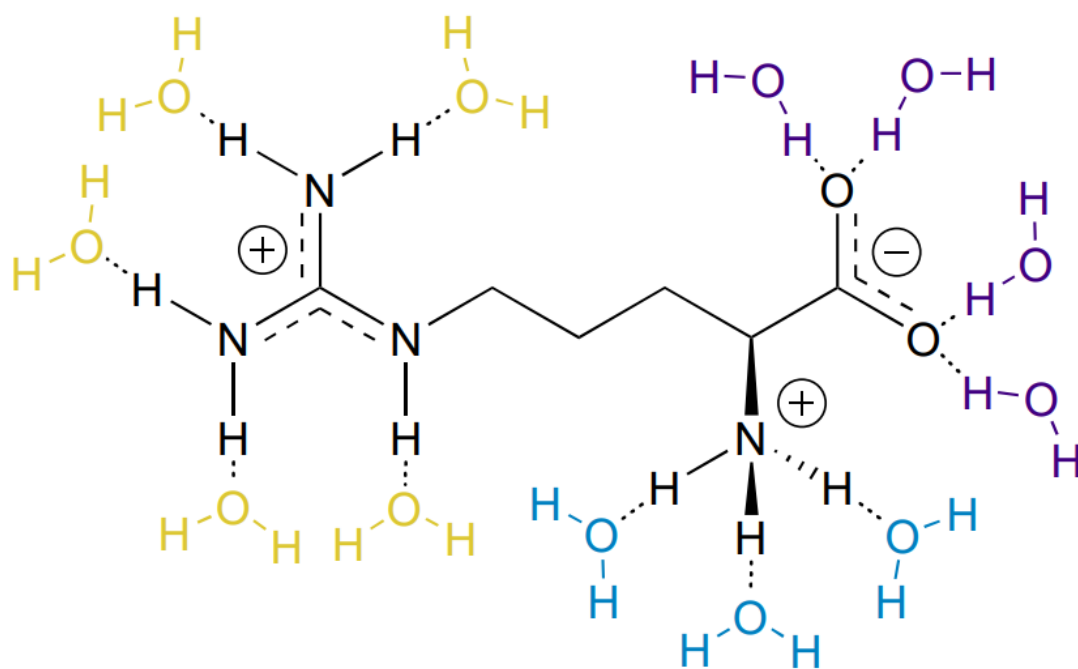


Figure S9: Illustration of arginine-water hydrogen bond interactions. Water molecules interacting with the Gdm<sup>+</sup> sidechain are highlighted in yellow, while those interacting with NH<sub>3</sub><sup>+</sup> and COO<sup>-</sup> are shaded in blue and purple, respectively.

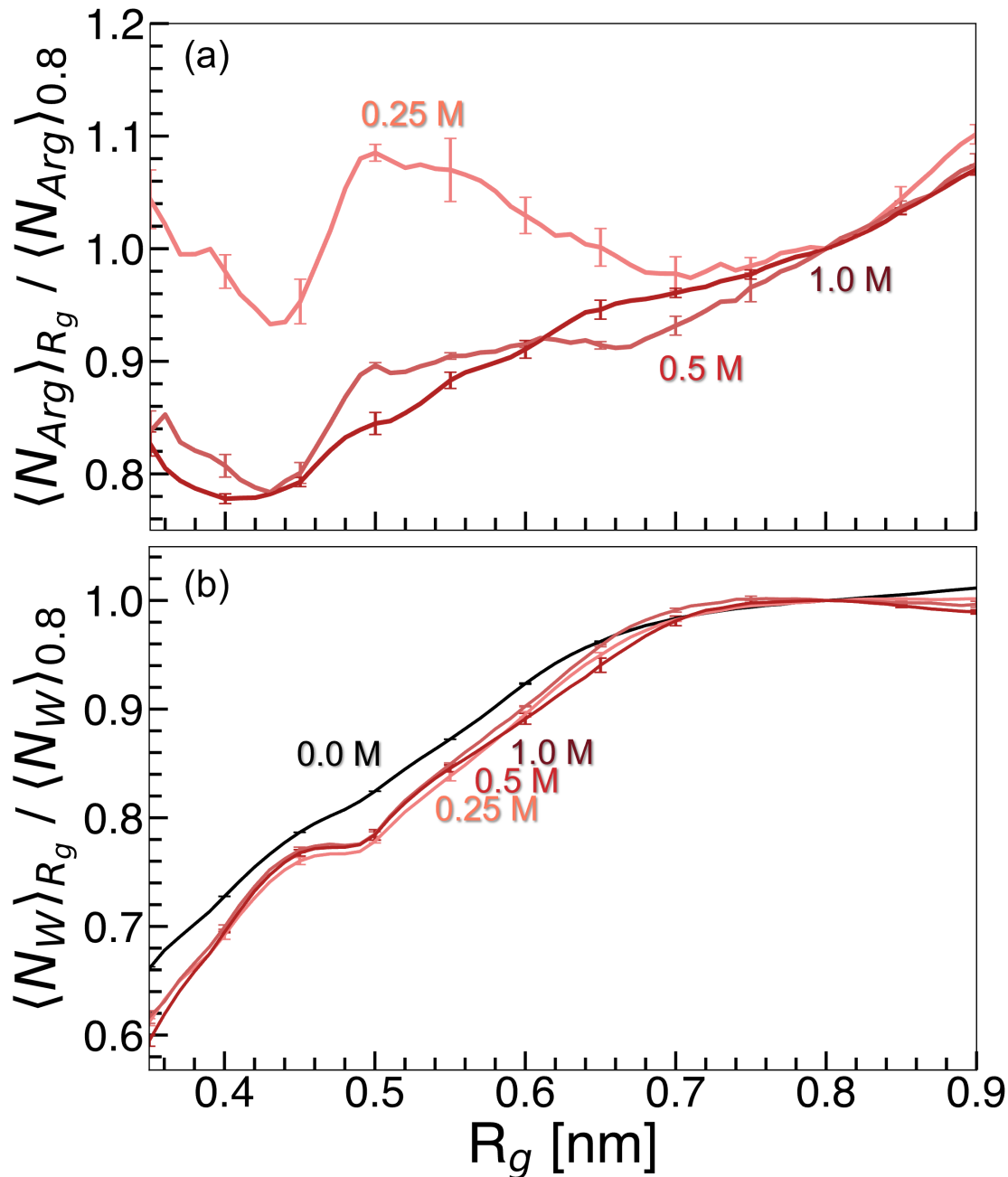


Figure S10: Quantification of arginine molecules and water molecules in the local domain of the hydrophobic polymer (within 0.5 nm). (a) Average number of arginine molecules in a given  $R_g$  window. (b) Average number of water molecules in a given  $R_g$  window. Values are normalized by the average value obtained at  $R_g = 0$  nm. Means are estimated as the average value in a given bin for three replicate REUS simulations. Concentration is denoted by increased shading (light to dark).

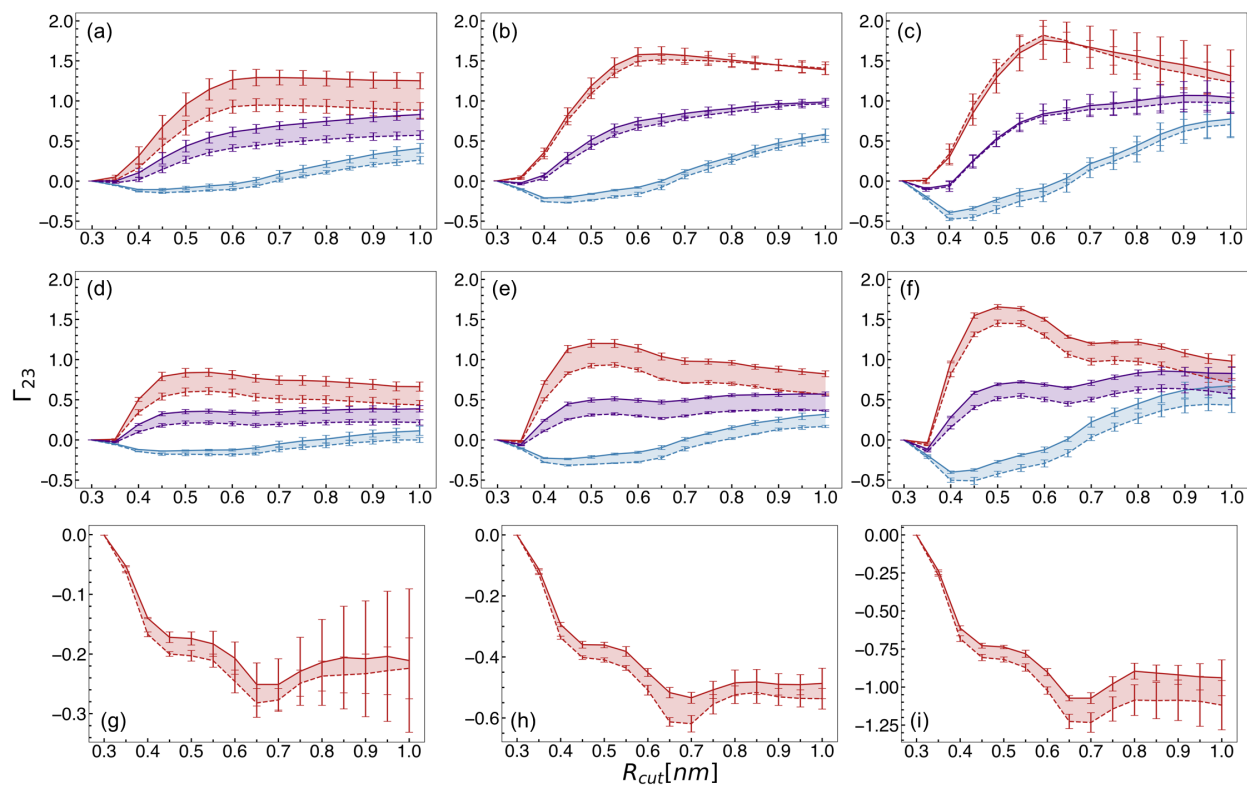


Figure S11: Preferential interaction coefficients for (a-c) arginine, (d-f) guanidinium, (g-i) glycine solutions. The additive is colored in red, counterion (if present) is colored in blue, and the net preferential interaction coefficient is colored in purple. Dashed lines indicate values for the unfolded state, while solid lines denote the folded state. Increasing arginine concentration is denoted by increased shading (light to dark). Mean values are reported from three replicate REUS simulations. Error bars were estimated as standard deviations from three replicate simulations.

## References

- (1) Abascal, J. L. F.; Vega, C. A general purpose model for the condensed phases of water: TIP4P/2005. *J. Chem. Phys.* **2005**, *123*, 234505.
- (2) Brooks, B. R.; Brooks, C. L.; Mackerell, A. D.; Nilsson, L.; Petrella, R. J.; Roux, B.; Won, Y.; Archontis, G.; Bartels, C.; Boresch, S. et al. CHARMM: The biomolecular simulation program. *J. Comput. Chem.* **2009**, *30*, 1545–1614.
- (3) Lorentz, H. A. Ueber die Anwendung des Satzes vom Virial in der kinetischen Theorie der Gase. *Annalen der Physik* **1881**, *248*, 127–136.
- (4) Bussi, G.; Donadio, D.; Parrinello, M. Canonical sampling through velocity rescaling. *J. Chem. Phys.* **2007**, *126*, 014101.
- (5) Berendsen, H. J. C.; Postma, J. P. M.; Van Gunsteren, W. F.; DiNola, A.; Haak, J. R. Molecular dynamics with coupling to an external bath. *J. Chem. Phys.* **1984**, *81*, 3684–3690.
- (6) Evans, D. J.; Holian, B. L. The Nose–Hoover thermostat. *J. Chem. Phys.* **1985**, *83*, 4069–4074.
- (7) Parrinello, M.; Rahman, A. Polymorphic transitions in single crystals: A new molecular dynamics method. *J. Appl. Phys.* **1981**, *52*, 7182–7190.
- (8) McInnes, L.; Healy, J.; Astels, S. hdbscan: Hierarchical density based clustering. *JOSS* **2017**, *2*, 205.
- (9) Record, M.; Anderson, C. Interpretation of preferential interaction coefficients of non-electrolytes and of electrolyte ions in terms of a two-domain model. *Biophys. J.* **1995**, *68*, 786–794.
- (10) Shukla, D.; Trout, B. L. Interaction of Arginine with Proteins and the Mechanism by Which It Inhibits Aggregation. *J. Phys. Chem. B* **2010**, *114*, 13426–13438.

- (11) Schneider, C. P.; Trout, B. L. Investigation of Cosolute-Protein Preferential Interaction Coefficients: New Insight into the Mechanism by Which Arginine Inhibits Aggregation. *J. Phys. Chem. B* **2009**, *113*, 2050–2058.
- (12) Schneider, C. P.; Shukla, D.; Trout, B. L. Arginine and the Hofmeister Series: The Role of Ion–Ion Interactions in Protein Aggregation Suppression. *J. Phys. Chem. B* **2011**, *115*, 7447–7458.
- (13) Vagenende, V.; Han, A. X.; Mueller, M.; Trout, B. L. Protein-Associated Cation Clusters in Aqueous Arginine Solutions and Their Effects on Protein Stability and Size. *ACS Chem. Biol.* **2013**, *8*, 416–422.